HPT Annex 50

Heat Pumps in Multi-Family Buildings

Task 3.2: System Simulation

Country Report

AUSTRIA

Edited by Graz University of Technology   R. Pratter, W. Lerch, R. Heimrath, R. Rieberer
Contact: rene.rieberer@tugraz.at

June 30, 2020 (Version 1)

Contents

Summary

The Austrian contribution to the IEA HPT Annex 50 - Task 4 (Demonstration) deals with the monitoring of an existing multi family building located in Weiz (Austria). The heating system uses an ice storage and solar collectors as heat source for two brine/water heat pumps and delivers heat to the space heating and domestic hot water system.

Within Task 3.2 a TRNSYS model of the overall system has been set up, and validated with measurement data. The quality of the model was judged sufficiently accurate for a simulation based analysis of different modifications of the real system, e.g. variation of the ice storage volume or/and the solar collector area. Finally, a theoretical comparison of the realized system configuration with a system using an "advanced" air/water heat pump was carried out. The model of the air/water heat pump is a result of the Austrian activities within Task 3.1.

It turned out that some room for improvement exist for the system in Weiz. Especially a larger heat source system (ice storage and/or solar collector) would be beneficial with respect to efficiency and energy consumption. However, due to economic reasons no optimization of the hardware has been realized up to now.

1   Introduction

This report deals with the system simulation of a solar-ice storage-heat pump system. The analysed system is a multifamily building which is located in Weiz (Austria). This report is mainly based on the Master thesis of Pratter (2017) and the results of the project "Hot Ice" which was financially supported by the province of Styria (Pratter el al., 2017). "Hot Ice" focuses on the use of latent heat with two ice storages and two heat pumps in combination with unglazed solar collectors and a PV system. It was designed as a pilot project for local heat supply.

The main components, its operating modes and the monitoring of the system are explained in detail in the report on Austrian HPT Annex 50 – Task 4 (Task 4 report). However, here follows a brief description of the system.

The construction of the MFB (multi-family building) which is located at Bärentalweg 6 in 8160 Weiz was finished in April 2015. The building, shown in Figure 1-1, is a wood frame construction which accommodates ten different apartments on three floors. The total area adds up to 1477 m^2, whereof an area of 957 m^2 is heated. It fulfils the passive house standard and has a calculated thermal heat demand of 9.91 kWh/(m²a).

Figure 1-1 Building in Weiz (Hutter, 2016)

Figure 1-2 shows the hydraulic scheme of the heating system which is used in this building. A more detailed description of the most important components can be found in the Task 4 report.

As shown in Figure 1-2, the heat provided from the solar collector can either be used to charge the ice storage via a heat exchanger or as heat source for heat pumps. It is impossible to use the heat from the solar collector directly to heat the domestic hot water (DHW) or the space heating (SH) storage because the temperature is too low and must be lifted to a higher level by the heat pumps before. Depending on the current heat demand, one or two heat pumps are in operation. They always work in one mode (DHW or SH storage) and ensure that the temperatures in the storages remain within the desired ranges. Instead of the solar collector, the heat pump can also use the ice storage as heat source. If both heat sources are not sufficient, there is a further possibility to heat the two storages with an auxiliary heater. During the summer, this system can also be used for cooling. For this, the ice storage is used directly as heat sink ("cold source"), so that no additional chiller is needed.

Furthermore, the building has a controlled ventilation system with heat recovery. With this ventilation system, it is possible to heat the supplied air. A more detailed scheme of the heating system including

the sensor positions for the measurement as well as the ventilation system can be found in the Appendix.
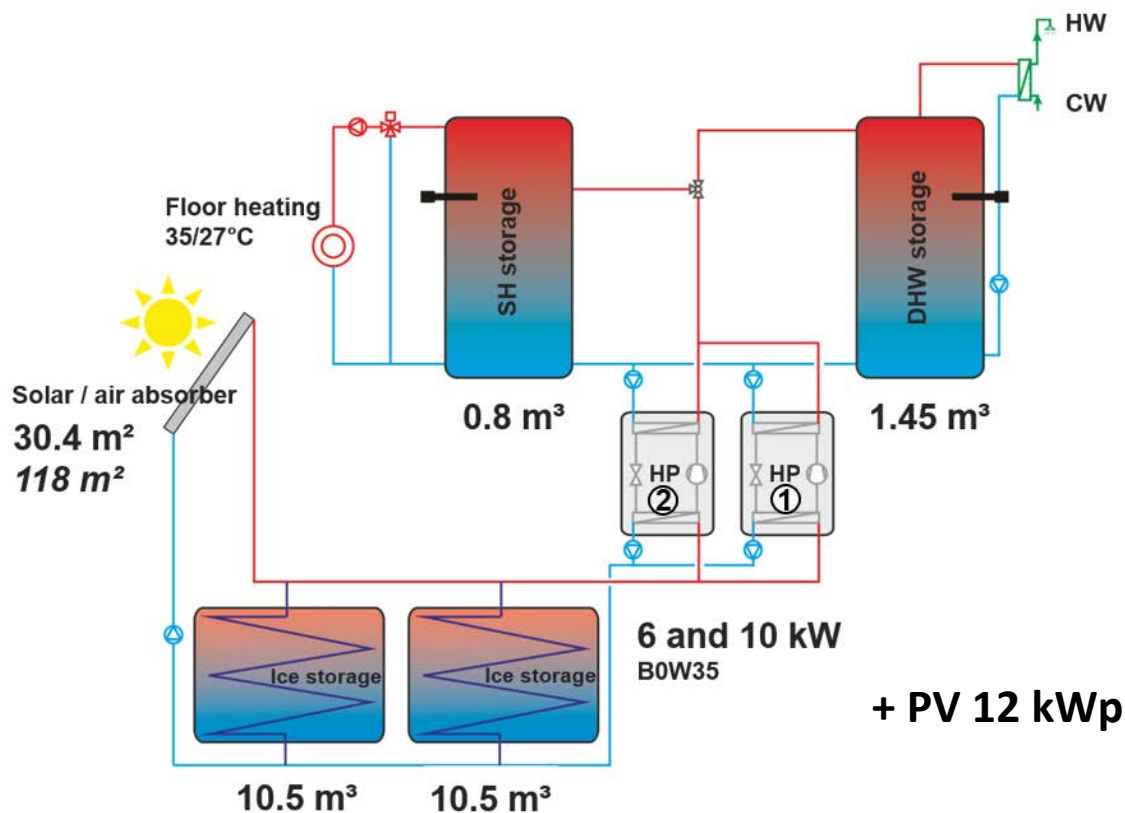
Figure 1-2: Hydraulic scheme (Lerch, 2017)

A significant number of measurement sensors has been installed, which allows a detailed analysis of the functioning of the system. Some of the most important sensors are the heat meters, which measure the inlet and return temperature as well as the flow rate. In addition, they also provide the thermal power and the heat quantity, which are calculated from the measured values and the fluid data: two for each heat pump (one for DHW and one for SH), one for the solar collector, one for cooling and one for the ventilation system. Furthermore, there are, for example sensors to measure the collector temperature, the global radiation, the ambient temperature, the electric power of the heat pumps and the electric heating elements to mention only some of them. Moreover, several sensors are installed to measure the ice storage and the surrounding soil temperatures.

The data of these sensors are not only recorded for later analysis, but can also be viewed using the HMI App (HMI-Master GmbH, 2017). This app visualizes the current system status. It is, therefore, possible to observe at any time in which operating mode the system is currently working, how high the storage temperatures are, or whether a problem occurs somewhere. In addition, all electrical and all heat quantity meters as well as the current weather data are displayed. Furthermore, the temperatures, CO_2 concentration and relative humidity in each apartment can be observed. This makes the app a valuable tool for monitoring and better understanding the functioning of the system.

2 Modelling and simulation of components and systems

Based on the system in Weiz a simulation model was developed in TRNSYS (2012). This model was validated with the measurement data of the year 2016 to ensure that the model corresponds to the real system as good as possible. The validated model was used to test some possible improvements before realizing them in Weiz. Furthermore, the solar/ice storage-heat pump system was finally replaced by a fictive air/water heat pump in the simulation to allow a comparison of the different technologies.

2.1 Validation of the solar-ice storage- heat pump simulation model

This subchapter deals with the validation of the simulation model as well as with its fine-tuning by using the measurement data from Weiz. First, the solar collector, the ice storage and the ground model were validated with the measured data in order to compare the simulation model with the real system. Second, these components were integrated in the overall heating system model to validate this as well.

2.1.1 Validation of the single components

The validation of the single components was important because some main parameters, such as the characteristic curve of the solar collector, have not been disclosed. In addition, the ice storage model (Type 843) considers a rectangular storage with only one heat exchanger, while the real ice storage is cylindrical with a separate regeneration and extraction heat exchanger. To parametrize the ice storage model in such a way that it corresponds well to the real one, was one of the biggest challenges in validation phase.

2.1.2 Procedural method

For the validation, meaningful data ranges of the different operating modes (see Task 4 report) were selected from the available measured data. This data was selected as input for the respective model to be validated. As far as possible, one minute values were taken, as a larger number of measured data has a positive effect on the validation result. The known parameters were set as constants in the respective type, while the others were varied between defined limits. These should be selected in such a way that a minimum deviation is obtained between the simulated and the measured output data. By comparing several operating modes and data areas, it was tried to find the best configuration of the simulation model so that the behaviour was as realistic as possible.

2.1.3 The solar collector

The used collector model is Type 203 developed for unglazed photovoltaic-thermal (PVT) collector modules by Jansen Energieplanung. In the PVT collector model, the incident solar radiation is partly converted into electrical energy in the PV module. This share is no longer available for thermal use. Therefore, the usable radiation for the thermal part of the PVT collector is lower by the amount of energy, which is converted to electrical energy. This energy is still reduced by the infrared balance and then absorbed by the absorber. If the surface temperature of the collector drops below the dew point temperature of the ambient air, there is an additional gain of heat from condensation. Considering the losses, the useful energy can be determined. Figure 2-1 shows this energy flows of the collector type. (ISFH, 2011)
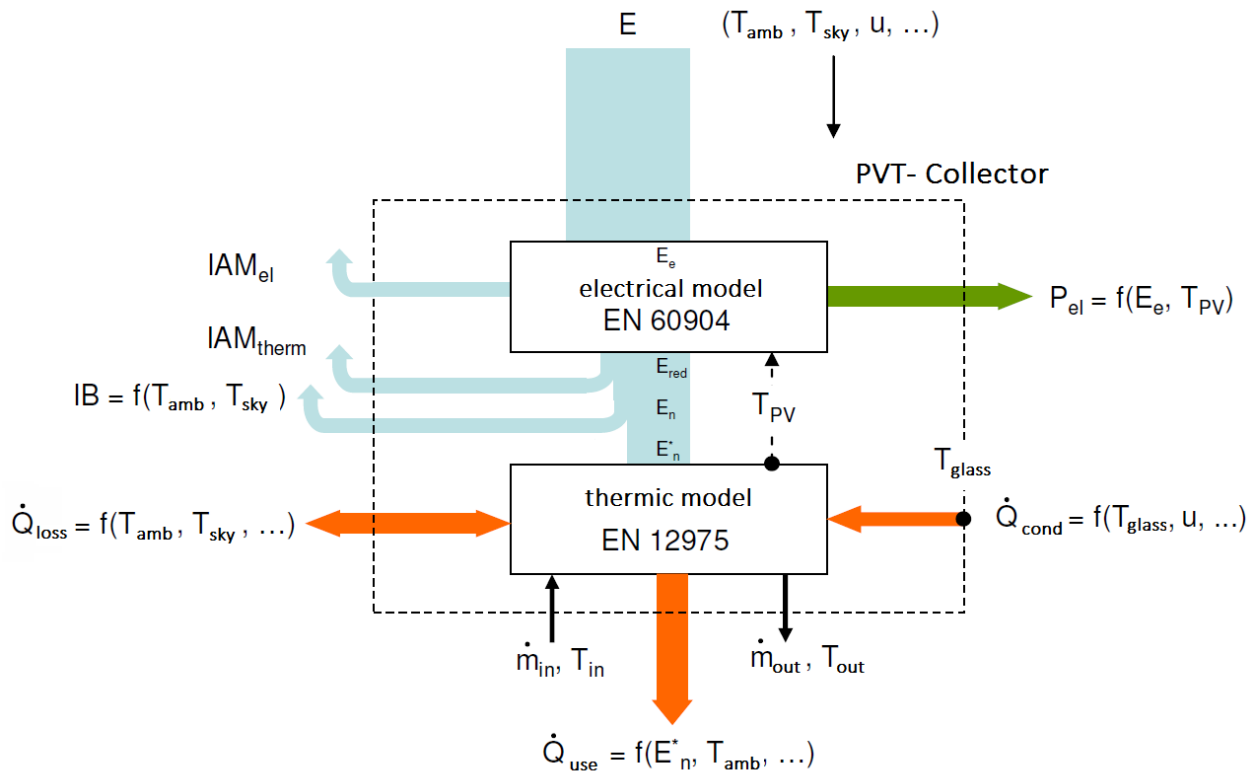
Figure 2-1: Energy flows of the collector type 203 (ISFH, 2011)

In Type 203, the thermal characteristic of the PVT collector is based on the non-steady collector model described in the standard EN 12975-2 for testing the performance of unglazed collectors. For the photovoltaic characteristic, there are two different models available: the "efficiency model" and the "effective solar cell characteristics model". (ISFH, 2011)

Since the installed collector is a purely thermal one, the simulation type operates in the corresponding operation mode. Concretely, this is mode 2 for the operation as a thermal collector with consideration of condensation. In Figure 2-1, only the orange marked energy flows are activated. In this case, the solar radiation is, of course, not reduced by the PV module, so that the whole radiation is available for the thermal collector.

Parameter setting

As far as possible, the parameters were taken from the data sheets or from other documentations (e.g., collector inclination, specific heat capacity of the fluid, etc.). However, the problem was that relatively little information was available. For this reason, some parameters were preliminary based on empirical values or assumptions.

The factors of the characteristic curve, the collector area and the heat capacity of the collectors were identified as the most important unknown parameters. For the characteristic curve, only the first two parameters, the conversion factor (a0) and the heat loss coefficient (a1), were used in the simulation

model. The "active" area of the collector was unknown because the installed collector was a two-layered one. This means that depending on the position of the sun, different levels of occlusion of the lower layer occurred. As the simulation type had only one layer, an equivalent area had to be found.

Implementation of the validation model in TRNSYS

To validate the solar collector, the collector model is considered isolated from the other components. The input data of the collector was provided from a data reader which reads, in predefined time intervals, the measured data from a text file. In an Equation Statement the necessary calculation were carried out, as for example the equation for the minimization in TRNOPT, see eq. (2-1). TRNOPT is a dedicated TRNSYS interface for GenOpt. It was created by TESS (TESS, 2012) to streamline the optimisation process and it is distributed as part of the TESS libraries Version 2.

$$\Delta E_{SimMeas}^2 = \sum abs(E_{Sim}^2 - E_{Meas}^2)$$
(2-1)

Therefore, the sum of the difference between measured (E_{Meas}) and simulated energy (E_{Sim}) is minimized in TRNOPT, by varying the already mentioned variables. In this case, the simulation runs in two stages. First, TRNOPT is started to find the optimal values of the parameters. This parameter must be set in the Equation Statement. Then the actual simulation is started in TRNSYS and the result is stored in the output file as well as displayed in the online plotter.

Chosen data range and the resulting findings

As input data, characteristic ranges of the individual operating modes (see Task 4 report) were used. Since a larger number of data was advantageous, the data from the one minute measurement intervals was selected because there were much more data available for the same period. In total, five cases were examined: two cases with the solar and two with the air absorber mode as well as one with the regeneration mode. For the "Heat pump with air absorber mode" the collector temperature is of course the lowest (once all the time below 0 °C and once under 3 °C). For the solar collector mode, it is up to 10 °C and for the regeneration mode, it is the highest.

In the first run the individual optimum values were searched for all cases. It turned out that it was no problem to find these values. The deviation between the simulated and the measured data was, after the settling time, in the per mill range. Figure 2-2 shows an example of the trends of the simulated and measured outlet temperatures which are nearly the same.
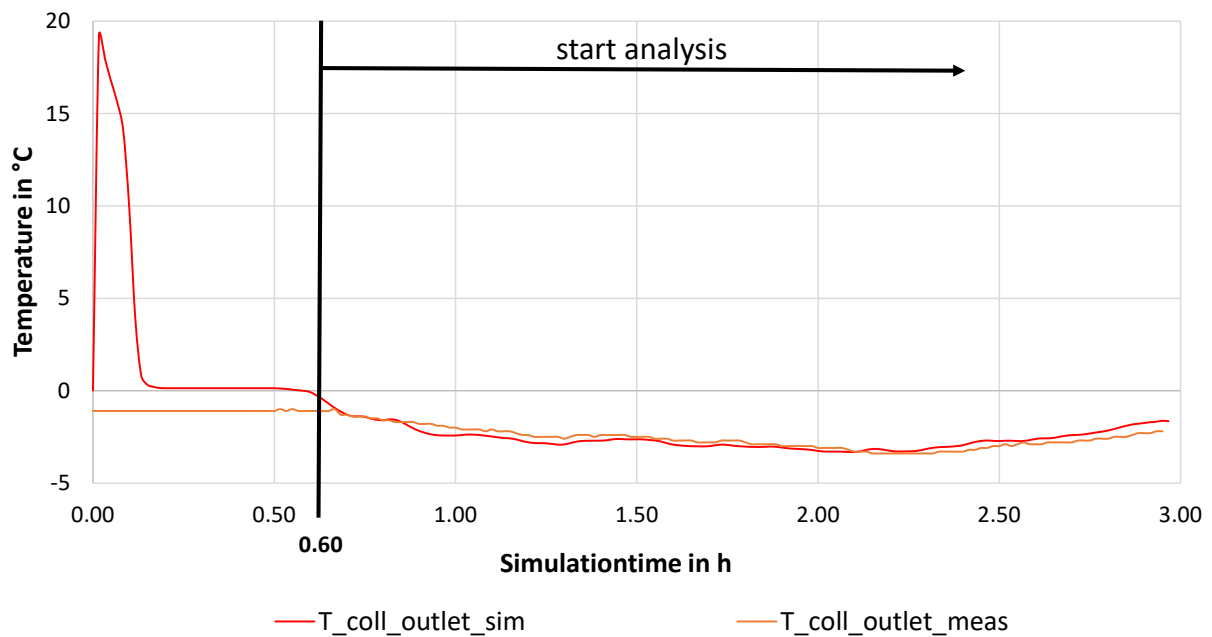
Figure 2-2: Simulation of one case with optimum values

Since the searched values are parameters and not inputs, a configuration should be found that satisfies all cases sufficiently. If this is not feasible as little as possible configurations should be made since they must be integrated via an additional collector model and a control which switches between them. The necessity of several collector models was considered because the simulation model is not a two-layered system, as it is the case with the actually installed collector. With this, the reduction of the area by the overlapping in the case of solar radiation could be considered, if necessary. Therefore, all cases were simulated again with the same configuration. It was found that the configuration of the regeneration sample fulfils the other cases well, so that no additional collector model had to be installed. Table 2-1 shows the mean temperature difference between the simulated and the measured outlet temperature in the optimum case according to TRNOPT and with the values optimal for the regeneration example. For this purpose, the absolute values of the temperature difference were considered after a settling time of 40 min. The temperature difference between the measured and the simulated temperature in case of the optimal values was, of course, lower, but one can see that the selected values did not cause much higher differences.

In addition to the temperatures, the heat quantity of the collector is important too. Therefore, in Table 2-1, the differences of the heat quantities between simulation and measurement are shown for both cases (optimum and regeneration). The heat quantities are again considered after 40 min of settling time. The magnitude of the deviation itself depends strongly on the duration of the considered case, which means that primarily the difference between the two cases is interesting. It is seen that the highest deviation occurs at case 4. Since with case 3, which has similar boundary conditions, a much better result was obtained, this deviation was not seen as a sufficient reason for a second collector model.

Table 2-1: Temperature und heat quantity differences between simulation and measurement for different cases and different parametrisation

	Case	ΔT_{Opt} [K]	ΔT_{Reg} [K]	ΔQ_{Opt} [kWh]	ΔQ_{Reg} [kWh]
1	Solar collector mode (04.02.2016 09:57 – 12:49)	0.60	0.68	3.12	3.51
2	Solar collector mode (05.02.2016 11:56 – 12:26)	0.38	0.60	0.28	0.53
3	Air absorber mode (29.01.2016 09:02 – 10:54)	0.62	0.77	1.53	1.99
4	Air absorber mode (01.02.2016 06:10 – 08:40)	0.29	0.36	0.14	1.47
5	Regeneration mode (01.02.2016 13:20 – 15:20)	0.29	0.29	0.22	0.22

Table 2-2 shows the chosen values of the determined parameters as used in the simulation of the overall system.

Table 2-2: Determined parameters of the solar collector

Parameter	Value	Unit
Conversion factor a_0	0.75	-
Heat loss coefficient a_1	42.5	$W/(m^2{*}K)$
Collector area A_{coll}	29	m^2
Heat capacity collector c_{coll}	40	$kJ/(m^2{*}K)$

2.1.4   The ice storage

For the simulation of the ice storage, Type 843, developed by TU Graz – Institute of Thermal Engineering (Institute of Thermal Engineering, 2017), was used. This model allows the simulation of a cuboid-shaped ice storage with an integrated pipe heat exchanger. It is very important to consider that during discharging an ice layer grows on the outside surface of the heat exchanger pipes, if the temperature is lower than 0°C. This layer of ice acts like an insulation layer and reduces the heat transfer between the liquid water in the tank and the heat transfer fluid in the heat exchanger pipes depending on the ice layer thickness. Ice formation and growth on the tubes and the increasing thermal resistance of the ice is considered by means of a finite difference formulation of the transient Fourier equation in cylindrical coordinates. For the modelling of the phase change from solid to liquid, the enthalpy method is used (Claußen, 1993; Visser, 1986). As a simplification, the temperature of the liquid water in the storage is assumed to be the same in the whole tank. (Lerch et al., 2016)

As shown in Figure 2-3, the heat exchanger is assumed as a pipe, which is laid in loops inside the storage. The pipe material, the diameter, the wall thickness, the pipe spacing distance and the number of the parallel cycles can be chosen as parameters. The heat exchange between the heat carrier fluid and the inner wall of the heat exchanger pipes is calculated using an empirical model for the flow in cylindrical pipes (VDI Wärmeatlas, 1997). The heat losses/gains of the storage to/from the ambient (soil in this case) are calculated through a heat loss coefficient UA_{Loss} [W/K] which is provided as an input. (Lerch et al., 2016)
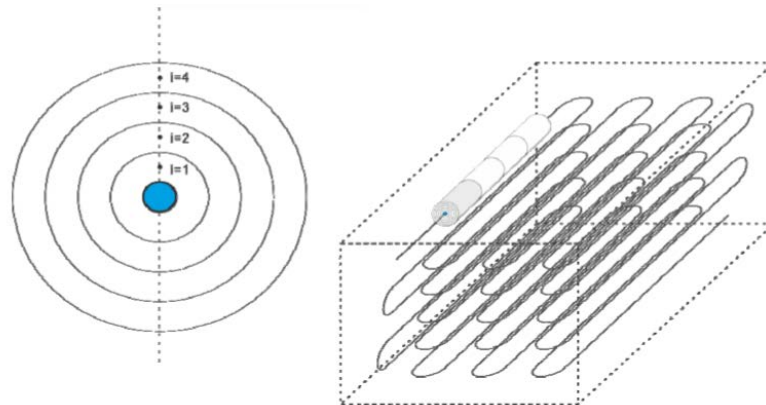
Figure 2-3: Schematic of the ice storage model for TRNSYS Type 843 (Cao et al., 2013)

Parameter setting

As for the parameterization of the solar collector, all known parameters were taken from the data sheets. The difficulty was that the simulation model was cuboid-shaped with only one heat exchanger, while the real ice storage was a cylinder with two heat exchangers. The volume and the height of the storage model were selected the same as the real storage. The same applied to most parameters of the heat exchanger as well as to the entire substance property data. The only parameter to optimize was the maximum distance between the two heat exchanger pipes, which also defines the maximum diameter of the ice cylinder.

Input data

The mass flow and the temperature of the fluid coming from the solar collector during the regeneration phase as well as the return temperature and mass flow on the side of the heat pump are required as inputs. These the values are measured by the heat quantity meter, respectively, in case of the temperature from the collector, it is the collector outlet temperature itself because the solar heat quantity meter measures the temperatures only in integers, which is not accurate enough. In addition, the ambient temperature around the ice storage (soil temperature) is required as a further input. This temperature is given by the ground sensor 1/2, which is placed on the outer storage wall (see Task 4 report).

Since the simulation model has only one heat exchanger, a solution had to be found, so that the simulation model correlated with the real storage as good as possible. The method to assume an alternate flow through the heat exchanger turned out not to be very realistic because the ice formed was immediately defrosted at the next regeneration cycle, which is not the case in reality. Therefore, it was decided to operate only the heat extraction from the ice storage (heat pump source side) with the heat exchanger of the simulation model. The regeneration, instead, was operated with the double port

which was also available in the simulation model. This means that the fluid flowed without a heat exchanger directly into the ice storage. Since the fluid in the solar collector was brine and the ice storage was filled with water, an external heat exchanger in front of the ice storage was required in the overall system model. (For the real system, such a solution would of course not be possible because it would no longer work when the phase transition starts. However, in the simulation model this solution achieved the best results.) For the validation, this means that the maximum distance between two heat exchanger pipes must be determined with the heat pump data. The external heat exchanger for regeneration was later validated together with the overall system.

Implementation of the validation model in TRNSYS

The procedural method for validating the ice storage is similar to that of the solar collector (see above). The ice storage is also separated from the other components. The idea of a common validation with the soil coupling (Type 708) was discarded because this did not work with TRNOPT. Since both ice storages are identical and are operated the same, the validation must be carried out only once.

In this case the absolute difference of the flow temperature of the ice storage unit between simulation and measurement was selected as the quantity to be minimized, eq. (2-2). This is calculated in the equation type, summed with the integrator, and then passed to TRNOPT for the optimization.

$$\Delta T_{SimMeas} = \sum abs(T_{Sim} - T_{Meas})$$ (2-2)

Chosen data range and the resulting findings

Since during the monitoring of the one minute interval the ice storage was never operated as source for the heat pump for more than a few minutes, the 15 minutes data had to be used in this case. A period with a duration of approximately 16 hours could be found, so that a meaningful validation was possible. The selected case is shown in Figure 2-4. Since the ice storage was in the phase transition, the simulation model had to be "transferred" to this condition via pre-simulation.
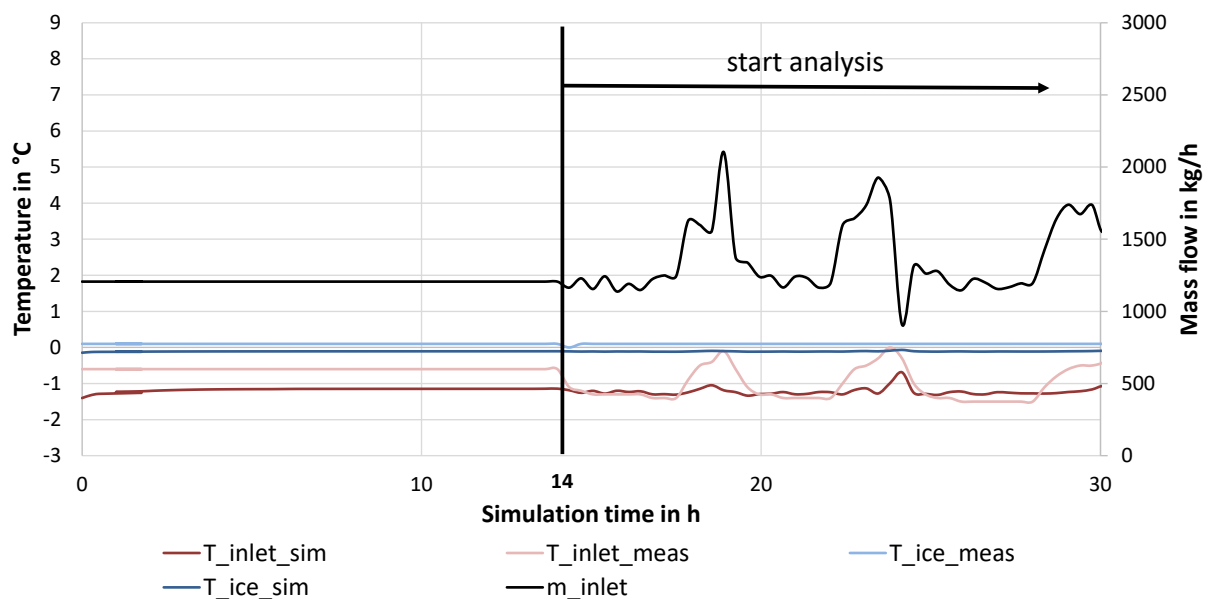
Figure 2-4: Validation of the ice storage model

For Figure 2-4, the optimum value of 14.7 cm for the distance between the heat exchanger pipes, determined by TRNOPT, has already been used. This is only valid for the extraction heat exchanger of the ice storage. The external heat exchanger for the regeneration is validated together with the soil coupling.

The peaks of the measured data are smaller in the simulation. However, the deviation in this range is only about 1 K. For the heat quantities, this results in a difference of 2.8 kWh (Q_{sim} = 33.4 kWh, Q_{meas} = 36.2 kWh). Since the validation of the ground type together with the ice storage type confirms the permissibility of this configuration too, the distance of 14.7 cm is also used for the simulation of the overall system.

2.1.5 Soil coupling

The used ground model (Type 708) maps the unsteady temperature field within a ground segment with an enclosed cistern. This type allows the coupling with external hot water storages as well as with ice storages. For this purpose, the storage fluid temperature is transferred to the Type 708 as input variable. The temperature calculated in Type 708 on the inner cistern wall surface and the cistern cavity are transferred again as input variables to the external storage model. There they form the boundary condition for the calculation of the thermal storage losses to the environment. The heat loss coefficient of the storage, which is crucial for this, is also used in Type 708 for the calculation of the temperatures. (Janßen Energieplanung, 2010)

The temperature field is assumed to be rotationally symmetric, therefore, the two-dimensional non-stationary temperature field is mapped in the radial and vertical directions. The model allows a differentiation of the thermal soil properties in both directions. On the surface of the ground, Type 708 considers the absorption of solar radiation and the heat transport to the environment by convection and heat radiation. The lateral boundary of the mapped soil segment is assumed to be adiabatic. For the lower limit, undisturbed soil is assumed. This temperature is to be specified as a parameter. (Janßen Energieplanung, 2010)

Parameter setting

To reproduce the soil with Type 708 correctly, a series of parameters is necessary: the parameters of the external storage model with its geometric dimensions, heat loss coefficients, etc. as well as the parameters of the soil itself. Figure 2-5 shows the geometric parameters which must be specified.
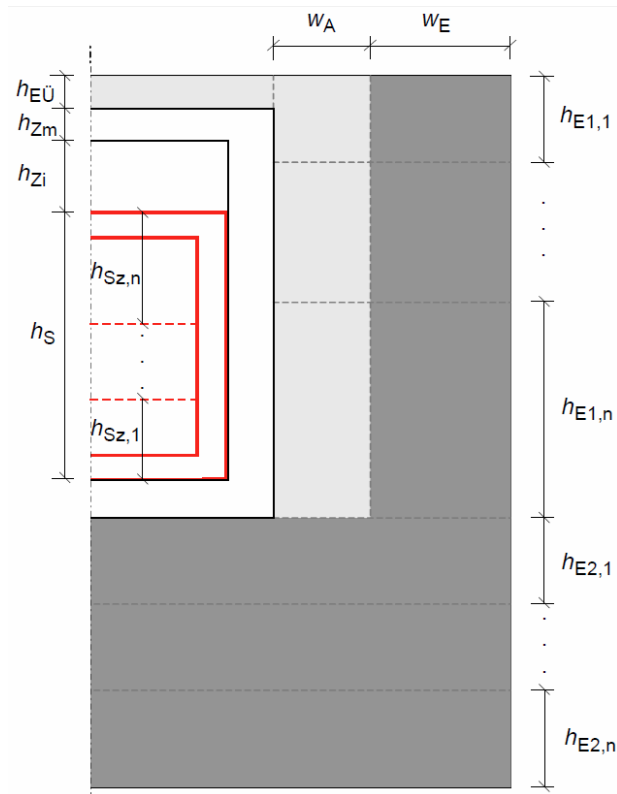
Figure 2-5: Geometric parameters of Type 708 (Janßen Energieplanung, 2010)

The storage height h_S, the cistern height h_{Zi}, the cistern wall thickness h_{Zm} and the overlap $h_{E\ddot{U}}$ must be specified in the vertical direction. While the storage height and the overlap were taken directly from the data sheets, the other two parameters were determined during the validation since the simulation model deviates slightly from reality. The storage is modelled as a mixed system with only one zone. The soil itself is divided into two zones in vertical direction, h_{E1} for the area next to the ice storage and h_{E2} for the area below. The second zone indicates the lower limit of the soil to be modelled and is selected in that way that the assumption "undisturbed soil" is fulfilled. In the horizontal direction, no differences in the soil in the proximity of the storage are assumed. Therefore, the soil is only calculated with one horizontal zone w_E.

Apart from the geometrical parameters, the heat loss coefficients play an elementary role. A distinction is made between the heat losses at the side walls, at the top and at the bottom of the storage. In addition, the heat transfer coefficient between the cistern surface and the storage top in the cistern cavity must be specified. These are together with the efficiency of the external heat exchanger for the regeneration of the ice storage the essential parameters to be determined during validation.

Furthermore, some climatic data, as the yearly average of ambient temperature, the amplitude of monthly averages of ambient temperature, the day number of the simulation start, etc. are needed. These data were determined by using the standard climate and adjusted accordingly to the simulation data.

Input data

First, the required variables to define the boundary condition at the ground surface were to be specified as input variables. These were the global radiation, the reflectance, the sky temperature, the ambient temperature and the wind speed. These inputs were generated by the weather data reader (Type 15-2) with the climatic data of Graz for the year 2016 (ZAMG, 2017). The data from Graz was chosen because this is the closest weather station to Weiz.

Furthermore, the material data of the soil as well as the temperature of the ice storage had to be specified. The material data of the soil was chosen constantly for the entire simulation period for dry clay soil and the temperature of the ice storage was given from the ice storage type.

Implementation of the validation model in TRNSYS

First, it was thought to validate the soil type together with the ice storage in a separate TRNSYS file, ahead of the other components. However, since an optimization with TRNOPT was not possible due to the programming of the type and moreover an isolated consideration did not yield to the best results, the soil was validated directly in the overall system. For this purpose, the overall system was set up in advance in such a way that the characteristic figures and the energy balances of the single components matched the measurement data as exactly as possible. More about this is described in chapter 2.2.

In addition, the discussed parameters of the soil type were varied in such a way that the ice storage temperature of the simulation matched with the measured as good as possible. The focus was primarily placed on the ice storage and not on the soil temperature, as this is ultimately the crucial factor for the simulation model to represent the real system well. After a few iterations, it was, thereby, possible to find a configuration which represented the system satisfactorily.

Resulting findings

As seen in Figure 2-6, the ice storage temperature in the simulation model matches very well with the measured one. The subcooling in January 2016 takes place exactly at the same time and to the same temperature level. The cool-down period in autumn and the phase transition period are also matched very well. Only the thawing after the phase transition occurs a bit faster in the simulation. Due to the fact that the other temperature sensors installed in the ice storage also differ from each other in this area, this slight deviation should not be serious.
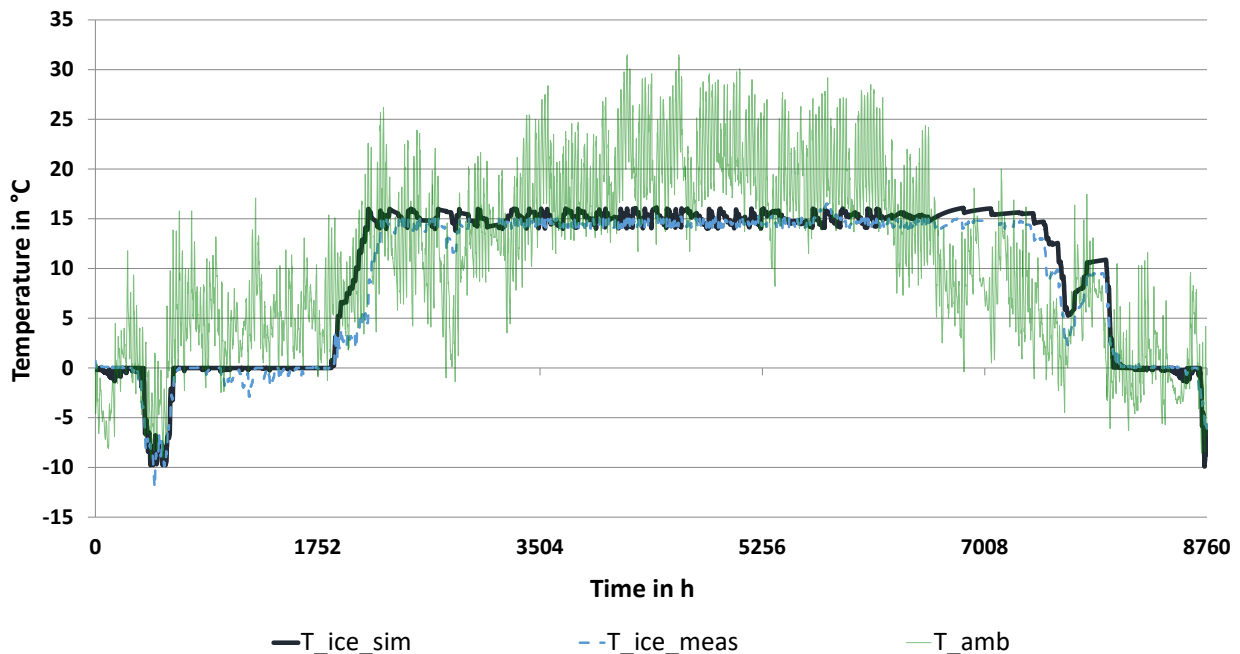
Figure 2-6: Trend of ice storage temperatures for the year 2016 (01.01 – 31.12)

2.2 The simulation model of the overall system

After the validation of the individual components, except of the soil model (Type 708) which was validated together with the overall system, their determined parameters were taken over in the overall system. This system model was setup by Lerch (2017).

The overall system was divided in three layers. The first layer includes the building (Type 56) and some necessary information like the ventilation, the internal loads as well as the weather data. The building was setup with TRNBUILD and designed in such a way that it correlated to the real building. Each apartment as well as basement and ground floor were designed as a separate zone. With the weather data reader, the according weather could be imported from a ".tm2 file". For the validation, the weather data from Graz for the year 2016 (ZAMG, 2017) was used, because this was the closest weather station.

Additionally, the printer which stores all important values for the evaluation in a one hour interval in a text file is placed here.

The second layer comprises the actual heating system and is the place where the validated components are installed. As determined in the validation, one solar collector model is sufficient to cover all operating conditions. As a result of the validation, the external heat exchanger was installed for the regeneration of the ice storages because of using the double port. The ground type is now connected to the ice storage and calculates the surrounding temperature (soil temperature). The built-in heat pump models are pure characteristic curve models which have been parameterized using the data sheets.

On the consumption side, the apartments were grouped into three zones to reduce the complexity. Therefore, the identical apartments were combined in each case. The apartments 1, 4, 5, and 8 were the

outlying apartments on the ground floor and on the first floor. The apartments 2, 3, 6 and 7 were the ones on the inside with an additional room for children and the apartments 9 and 10 were the bigger ones on the second floor. A plan of the building can be found in the Appendix.

It should be noted that the pipe losses were only considered in one heating circuit (apartment 9, 10) but for the entire pipe length. The domestic hot water requirement is depicted by a tap system, which receives a tap profile from an input file. This profile is based on the measured DHW demand for the validation. Here too, the pipe losses were considered. For the DHW and the SH storage, the same model (Type 340) but with different parameters was used. Both were non-stratified storages, which means that they had no stratified charging pipe but the naturally occurring stratification was calculated. They also considered the losses to the environment. In addition, in both storages an electric heating element was included which was activated when the ice storage temperature dropped below -10 °C.

The control of the simulation system is designed in such a way that it corresponds to the real system (compare Task 4 report). The only exception of this is the operation of the heat pumps. While in the real system sometimes only one of the two heat pumps is in operation, they operate always in parallel in the simulation model, which means that one heat pump never works alone. This simplification had to be made because the real control algorithm was unknown.

The already mentioned "Printegrator" is a combination of an integrator and a printer and is used for the output of all energies. These energies will be issued on a monthly base to compare them with the monthly balance sheets during the validation process.

The third layer contains some further types for the control of the system. These are mainly hysteresis controllers, which regulate the storage temperatures or the activation of the auxiliary heater.

2.3   Validation of the overall system

In order to ensure that the simulation model provides reliable results in comparison to the real system, a validation of the overall system was necessary in addition to the validation of the single components. For this purpose, the system was adjusted in such a way that the specific SH demand and the specific DHW demand matched with the measured data. Moreover, the measured and simulated ice storage temperature should also match as good as possible. Finally, the energy balances of the individual components, such as the solar collector, the ice storages, and the heat pumps, were compared with each other as well.

The parameters to be determined were the room temperature, the window ventilation and the shading as well as the already described validation of the ground type (see chapter *2.1.5*), which was also carried out within the overall system.

In the simulation model for all apartments and rooms the same set temperature was used. This temperature was estimated from the measured data (T_{room_i}) by the equation (2-3).

$$T_{mean\_room} = \frac{T_{room\_1} * A_{room\_1} + T_{room\_2} * A_{room\_2} + \cdots + T_{room\_n} * A_{room\_n}}{\sum A_{room\_i}} \qquad (2\text{-}3)$$

Thus, a room size weighted average temperature value of all heated rooms was calculated. With the measured data for the year 2016 (only heating period), this resulted in a temperature of 22.7 °C. Due to the inaccuracy of the measurement and the fact that this was a simplification, it was decided that a variation of ±1 K was allowed. This means that this temperature was used as starting point and was varied between 21.7 and 23.7 during the validation.

The shading was modelled in such a way that it was activated when the set room temperature was exceeded. Then the radiation was reduced to 15 % of the value without shading. In addition, a certain percentage of standard shading was supposed by balconies or by manual activation of the shading system. This percentage (shd_{offset}, equation (2-4)) was also to be determined by the validation.

$$shd = shd_{offset} + i_{on/off} * (0.85 - shd_{offset})$$ (2-4)

Moreover, the infiltration through open windows v_{vent_window} was also determined in the course of the validation. Therefore this ventilation was varied within reasonable limits during the validation. The variable v_{vent_window} was further multiplied with a ramp function which is 0 between 22 and 5 o'clock and 1 all the other time. With this equation, the infiltration behaviour was simulated as realistically as possible.

These three parameters (T_{mean_room}, v_{vent_window}, shd_{offset}) gradually varied in several simulations to find the best configuration. The result is shown in Table 2-3.

Table 2-3: Validation result

T_{room_set} [°C]	v_{vent_window} [h^{-1}]	shd_{offset} [%]
23.7	0.155	32

Due to the relatively high energy consumption, these values are also quite high, but this was necessary to achieve a good match between the simulation model and the real system. This consistency and the deviations are analysed in more detail in the following sub-chapters.

It should be noted that the validation discussed so far relates only to the space heating mode (SH). The profile for the DHW requirement has already been adapted with respect to the measurement data, so no further validation is necessary.

2.3.1 SH and DHW demand

As shown in Table 2-4, a good match between the measured and the simulated values could be found in the validation. Since the measured values also contain the storage and pipe losses, these had to be added to the simulated values to ensure comparability. The considered pipe losses are the losses between the storages and the apartments as well as the losses between the heat pumps and the storages. Comparing the simulation values including the losses with those of the measurement, it is shown that the deviation is below 0.1 %. This is a great result for the validation concerning the specific demands.

Table 2-4: Specific demands (based on heated area)

	simulation	simulation incl. losses	measured
specific SH demand [kWh/(m^{2}a)]	26.64	30.74	30.71
specific DHW demand [kWh/(m^{2}a)]	20.09	27.37	27.36

In this case the specific demands are referred to the heated area of 957 m^2. The meaning of the magnitude of these values is discussed in Task 4 report. A comparison of the simulation to the measurement in absolute numbers for the year 2016 is shown in Figure 2-7. The left bars show the distribution how the energy is provided, and the right ones for what it is used.
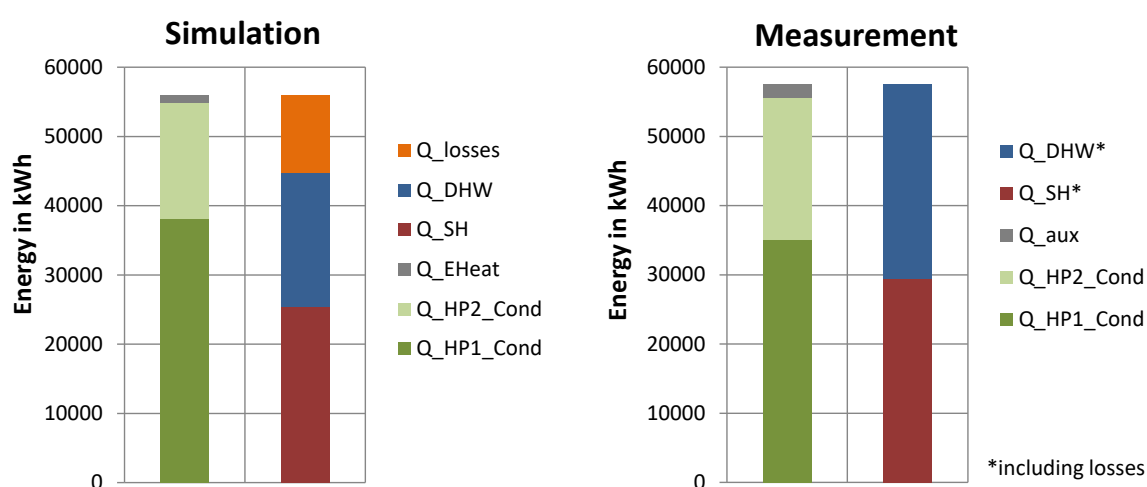
Figure 2-7: Total energy demand (01.01.2016 – 31.12.2016)

2.3.2   Ice storage temperature profile

The second indicator for the correct validation of the system was the ice storage temperature profile. In addition to the parameters discussed above, especially the ground model (type 708), which was also validated in the course of the validation of the overall system, was crucial for this. The result is shown in Figure 2-6 and has been already discussed in section 2.1.5. As shown there, a satisfactory result could also be achieved in this aspect.

It is also important to ensure that a pre-simulation is carried out, so that the ice storage temperature at the start of the actual simulation is consistent with the real data. Since during the phase transition it is neither known in the simulation nor in the real system how many percent of the storage is frozen, the duration of the pre-simulation was determined in such a way that the first sub-cooling occurred in both systems at the same time.

2.3.3   Balance sheets of the individual components

Despite the good conformity regarding the specific demands and the ice storage temperature profile, the simulation model differs slightly from the real system in some points. This is shown on the basis of the energy balances of the individual components. Each of them compare the measured values with the simulated ones for the year 2016.

Figure 2-8 and Figure 2-9 show the energy balances of the heat pumps. It can be seen that heat pump 1 provides more energy in the simulation than in the real system and that it is the other way around for heat pump 2. Due the fact that the precise control algorithm is unknown, which is why the simplification had been made that both heat pumps always operate simultaneously in the simulation model, deviations were expected at this point. In addition, the control of the real system has been modified during the considered year, which makes an exact comparison even more difficult. Since then, as can be seen in Figure 2-7, the overall energy of the two heat pumps together matched very well and the results have been classified as satisfactory.

Since the heat quantity of the ice storage as source for the heat pump was not measured and the solar heat quantity meter made many problems, the heat quantity on the evaporator side was calculated as the difference of the heat quantity on the condenser side and the electric energy consumed by the compressor. Consequently, the losses occurring at the heat pump cannot be considered.
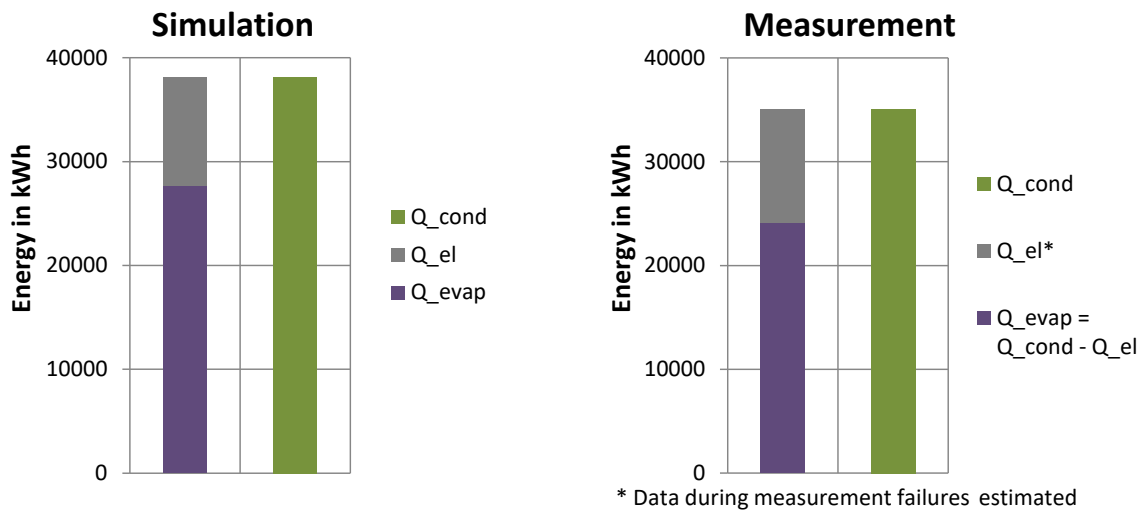
Figure 2-8: Heat pump 1 (2016)
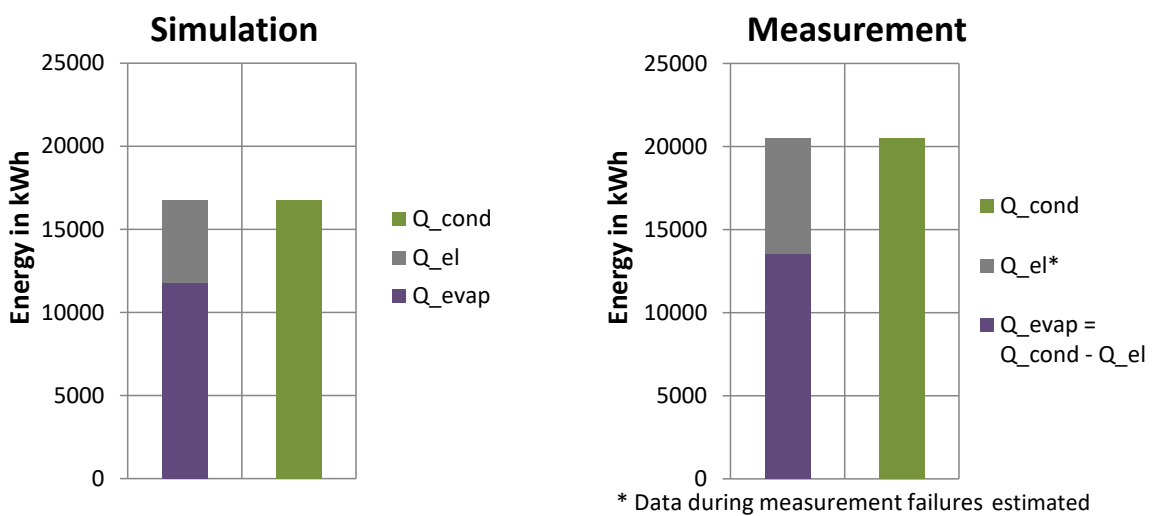
Figure 2-9: Heat pump 2 (2016)

The most significant difference between the simulation and the measured data appears for the ice storage. Figure 2-10 shows that the ice storage is much less used in the simulation model than in the real system. Since the ice storage temperature profile matches very well, the assumption is made, that the difference occurs during the summer months, when enough energy is available to reheat the ice storage immediately after use. One reason for this was a control error, which is why the SH storage temperature was maintained at 60°C throughout the whole summer. This energy is mainly supplied by the ice storage, because during the summer the collector temperature is often too high to be used as source for the heat pumps.

The energy content of the ice storage (Q_store) between 01.01.2016 and 01.01.2017 was not measured but can be understood as the difference of the input and output side of the balance sheet.
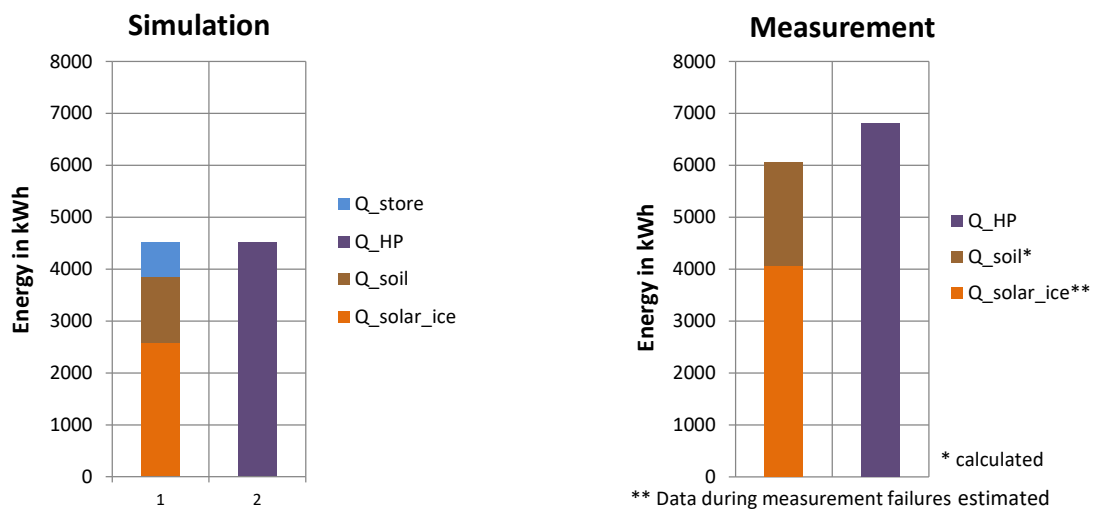
Figure 2-10: Ice storage (2016)

Figure 2-11 and Figure 2-12 show the energy balances of the DHW and the SH storage. Because of the reason that the system was validated concerning the specific SH and DHW demands, the balances had to match. As already mentioned, the losses in the measured data cannot be determined, which is why they are included in Q_DHW and Q_SH in the measured energy balance (system boundary condenser side of the heat pumps). Due to the size and the higher temperature level, the losses in the DHW storage are larger. Furthermore, it is shown that the energy demand of the auxiliary heating in the simulation model is slightly lower. The different distribution to the storages occurred because the auxiliary heating was activated in the real system only for the DHW storage.
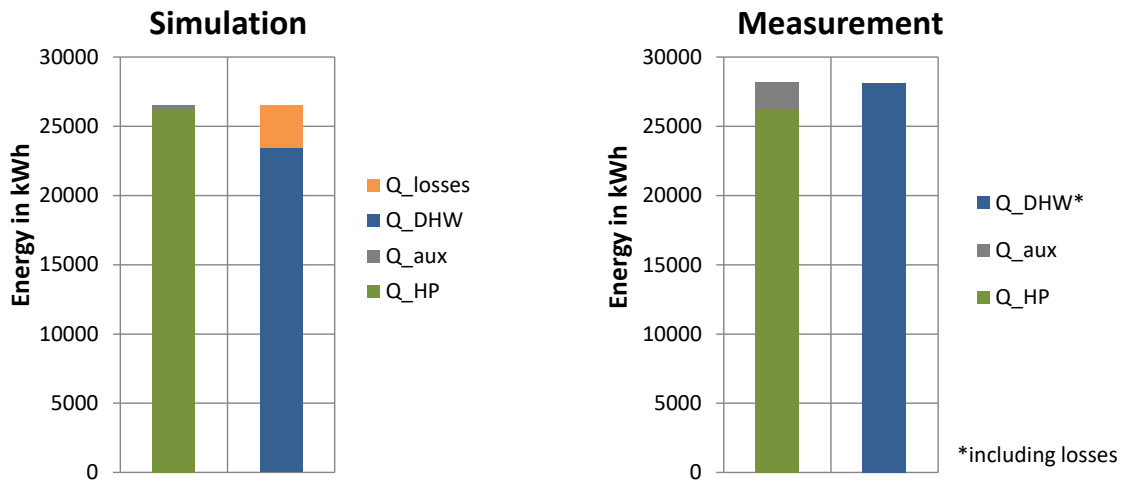
Figure 2-11: Domestic hot water storage (2016)

Figure 2-12 also shows the distribution of the heating energy to the single apartments according to the simulation model. It can be seen that the two apartments 9 and 10 (Q_SH910) in the second floor require more energy than the others. This is due to the fact that they are larger and located on the last floor, which means that in addition to most of the walls also the ceiling of these apartments is in contact with the environment.
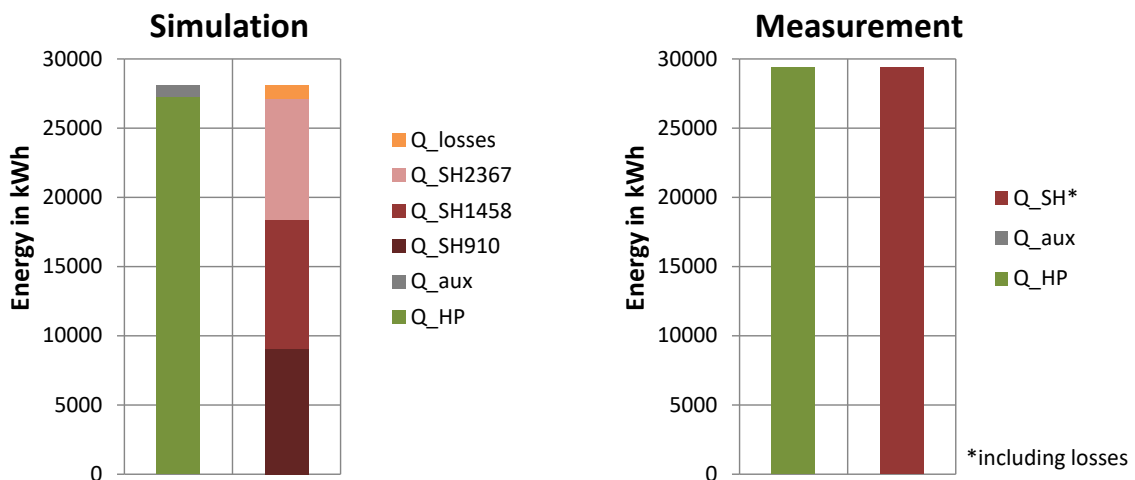
Figure 2-12: Space heating storage (2016)

Moreover, the balance of the solar collector (Figure 2-13) shows that the solar collector is more often used directly as source for the heat pump in the simulation, than in the real system. Because of numerous failures in the measurement of the solar data, as well as the fact that no data was available in

January, the measurement data is here rather to be understood as a rough estimation. That is why an analysis of the difference between measurement and simulation is dispensed with.

*Data during measurement failures were estimated
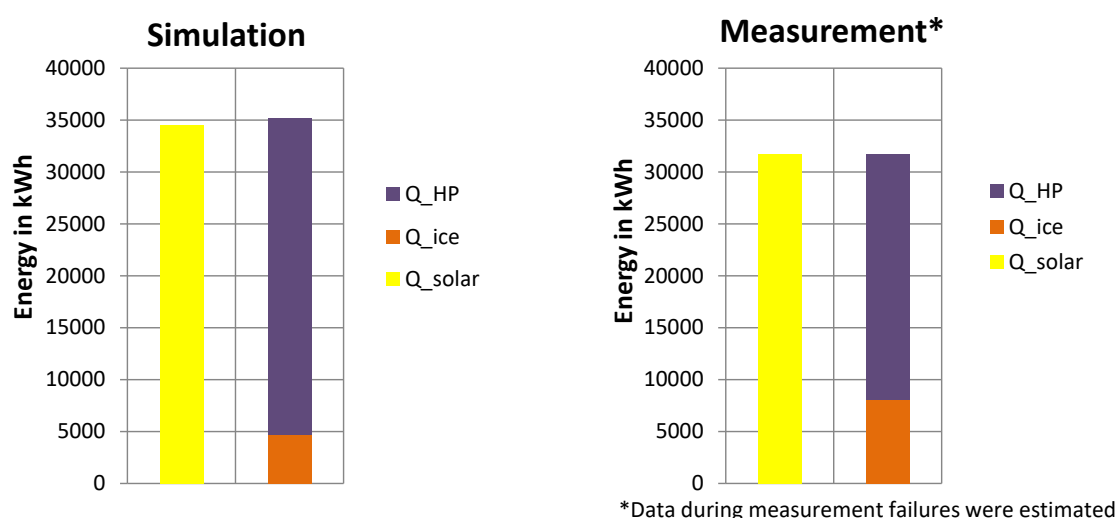
Figure 2-13: Solar collector (2016)

2.3.4 System Performance Factor

It is interesting to compare the SPFs between measurement and simulation. Table 2-5 shows that significantly higher SPFs of the heat pumps are achieved in the simulation model. This is possible due to the characteristic model of the heat pumps used. However, it is also a strong indicator that in the optimization of the system a collective mode of operation of the heat pumps, as used in the simulation model, should be examined more closely. Especially in view of the regeneration time (more time for the regeneration available because of shorter working times of the heat pumps) that could have a positive influence.

$$SPF_{HP,i} = \frac{Q_{cond\_HP,i}}{W_{el\_HP,i}} \quad i = 1, 2 \tag{2-5}$$

$$SPF_{HP\_mean} = \frac{Q_{cond\_HP1} + Q_{cond\_HP2}}{W_{el\_HP1} + W_{el\_HP2}} \tag{2-6}$$

Table 2-5: System Performance Factor

	Simulation	Measurement
SPF HP1	3.65	3.32
SPF HP2	3.39	2.96
SPF mean	3.57	3.19
SPF System	2.67	-

Furthermore, one can see that the SPF of the overall system according to eq. (2-7) is much lower than the SPF of the heat pumps. This SPF considers the electrical consumption of the heat pumps, the auxiliary heaters as well as all other pumps in the system shown in Figure 2-14. Since the share of the auxiliary heating (eq. (2-8)) is with 1.9 % not too big and the other pumps also need not much electric energy (287.5 kWh/a), this is mainly because of the high heat losses in the pipes as well as in the SH und DHW storage, which are also considered because of referencing the SPF$_{System}$ to the effective energy.

$$SPF_{System} = \frac{Q_{eff\_SH} + Q_{eff\_DHW}}{Q_{el\_HPs} + Q_{el\_pumps} + Q_{aux}} \qquad (2\text{-}7)$$

$$EHeat = \frac{Q_{aux}}{Q_{cond\_HP1} + Q_{cond\_HP2} + Q_{aux}} \qquad (2\text{-}8)$$
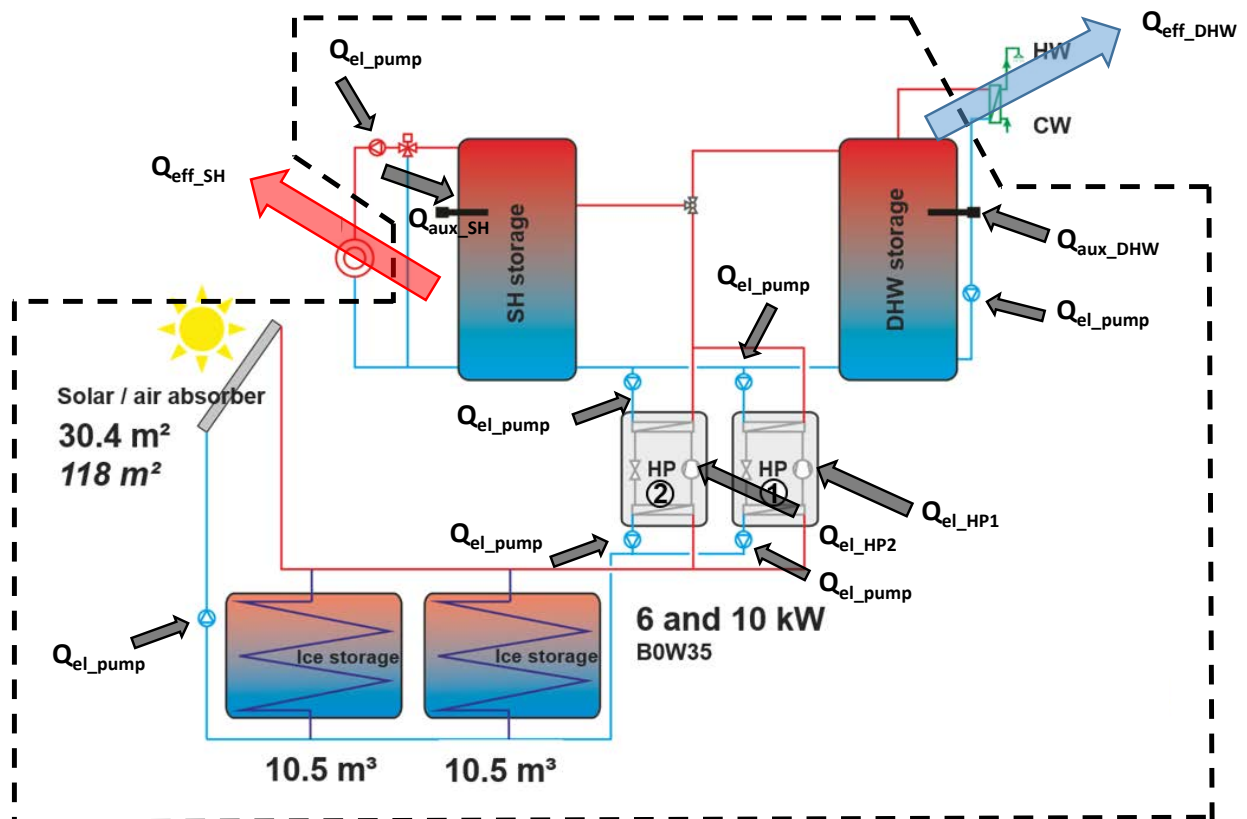
Figure 2-14: Energy flows for calculating the SPF$_{System}$

3   Simulation and investigation of possible improvements

In this chapter several potential improvements of the system are examined by modifying the validated simulation model. In the first step the ice storage volume and the solar collector area are increased and the inclination angle of the solar collector is varied. Additionally, bigger chances have been considered by installing a second solar collector. Different collector types (covered solar collector, evacuated tube collector) and different integration possibilities (heating the ice storage, direct DHW heating, etc.) have been investigated. The effects are explained in the following paragraphs.

All simulation results are related to the climate data of the location in Weiz for the year 2016. Since the simulation results are compared to the results of the validated system in the following figures, the comparison of the validated system with the measurement data should be made too. Therefore, the ice storage temperature of the validated simulation model and the measured temperature as well as some characteristic key figures are shown in Figure 3-1. As one can see, the trend of the two temperatures is quite similar whereby the biggest difference is the unfreezing in the spring, which happens faster in the simulation model. A detailed discussion of the result can be found in section *2.3.*
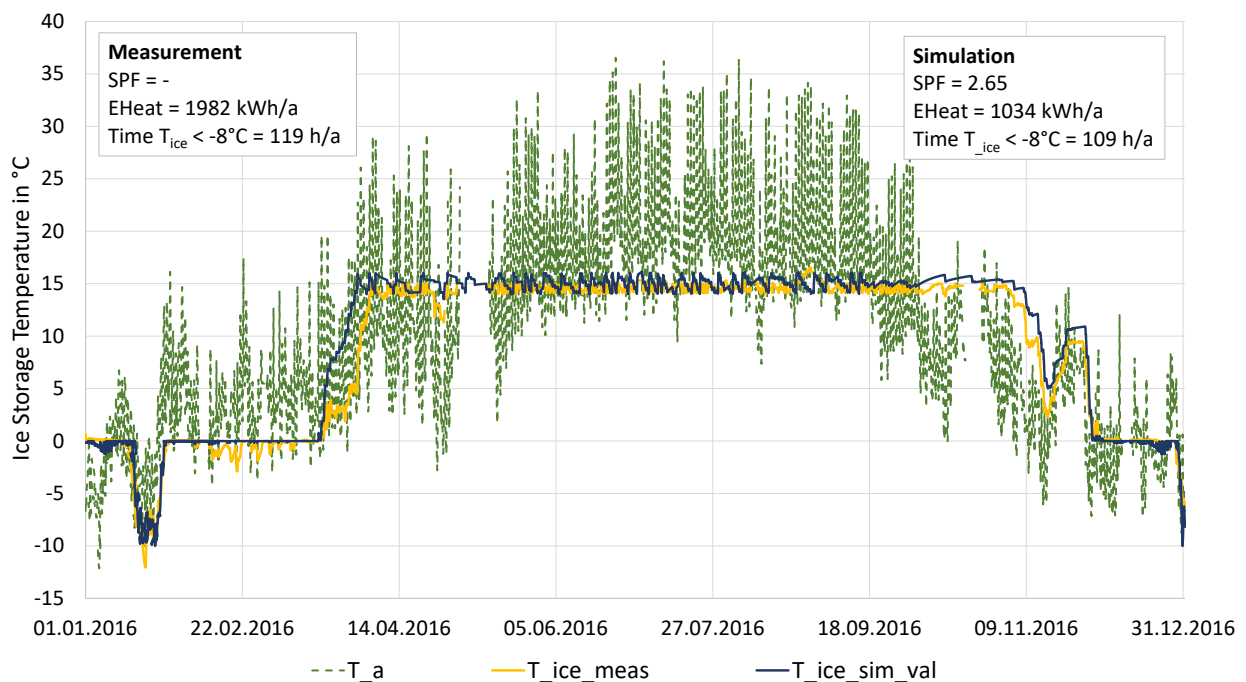
Figure 3-1: Comparison of the simulation result of the validated system with the measurement data

The following findings are based on Lerch (2017).

3.1   Variation of the component dimensions

In the course of the analysis the ice storage volume and the collector area have been increased originating from the validation result up to 150 % of it. The effects are shown in Figure 3-2. One can see that the necessary auxiliary heating decreases with an increase of the ice storage volume faster than with an increase of the solar collector area. With the climate data of 2016 no auxiliary heating would be necessary by increasing the ice storage volume about 40 %. A further enlargement does not have any positive influence anymore. The increase of the solar collector area has not such a strong influence on the necessary auxiliary heating, but a similar one on the SPF of the whole system. That is the case because the average flow temperature of the solar collector is increased too, which especially has a positive impact in case of using the collector directly as source for the heat pumps.
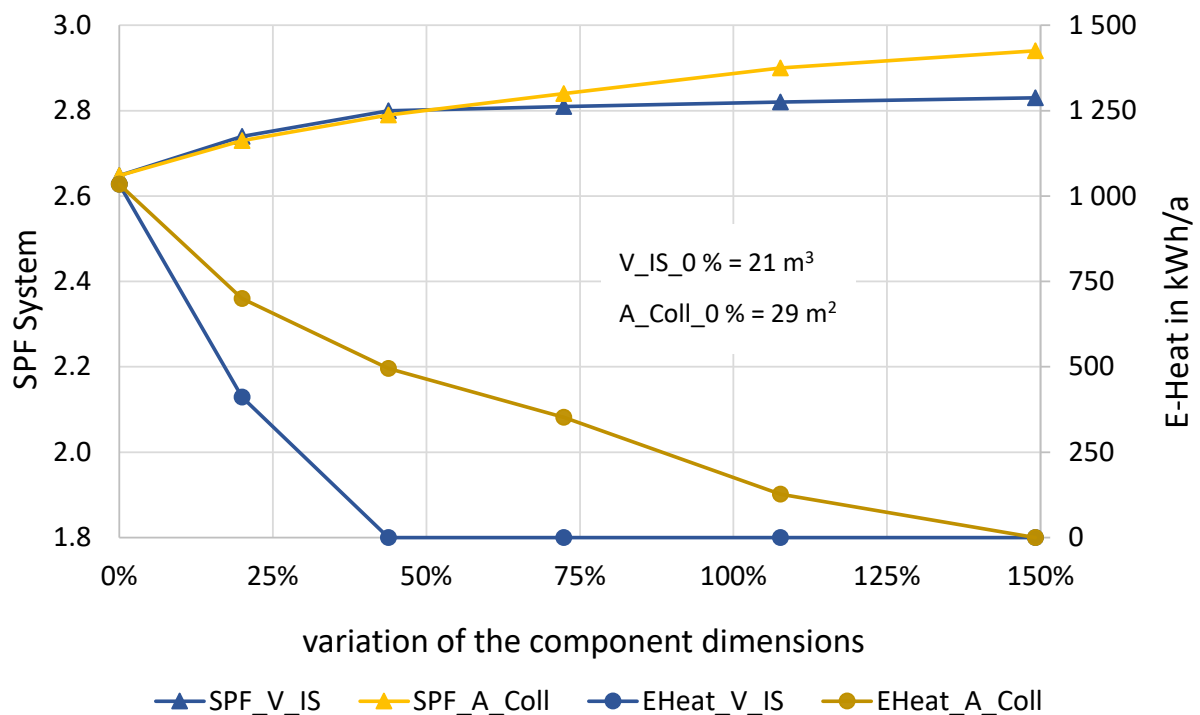
Figure 3-2: Sensitive analysis – enlargement of the collector area ("A_coll") and ice storage volume ("V_IS")

The ice storage temperature trend for the different ice storage volumes are shown in Figure 3-3 and in more detail in Figure 3-4 and Figure 3-5 for two selected cases. The difference is best seen in the period where the subcooling occurs and during the time when the ice storage is completely regenerated again. The bigger the ice storage is, the less is the time of subcooling, till no subcooling occurs anymore. However, it takes longer to regenerate the bigger ice storage.
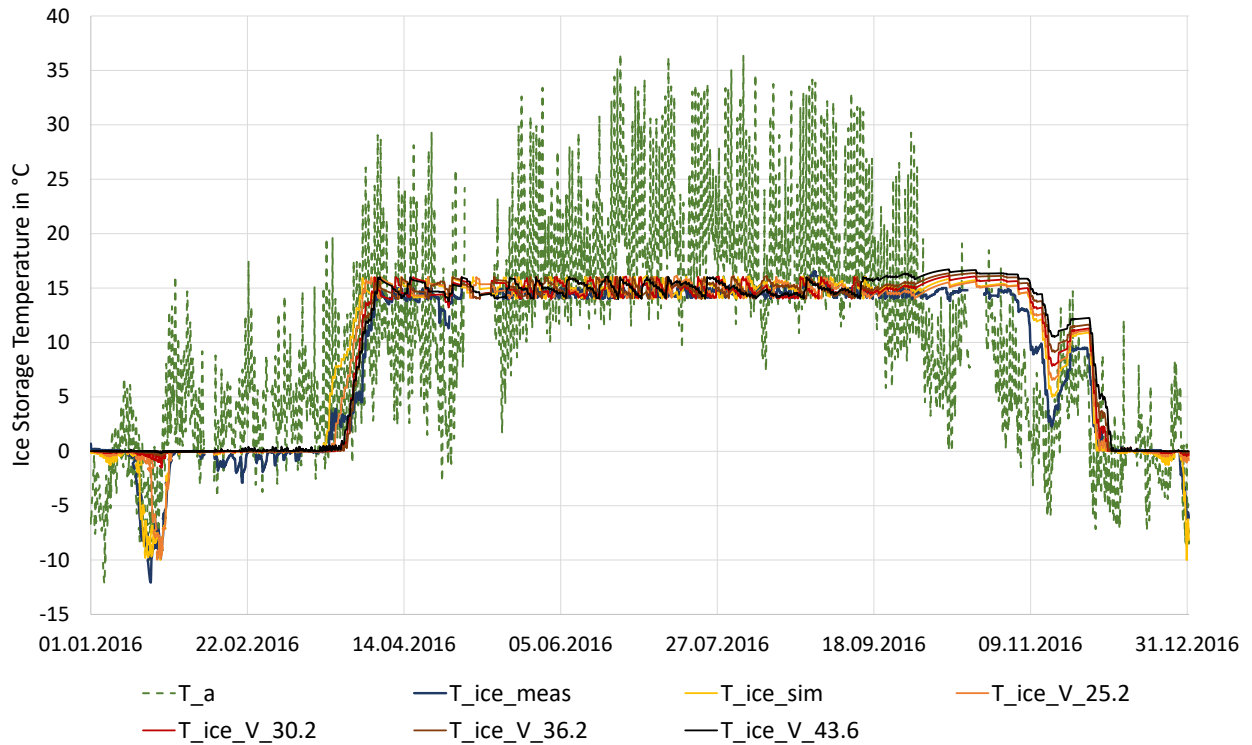
Figure 3-3: Ice storage temperature trend for different ice storage volumes
(Baseline: V_IS = 21 m³)

Figure 3-4 shows the ice storage with a volume of 25.2 m³ in comparison to the validated system (21 m³). It is seen that the increase of 20 % already reduces the hours of an ice storage temperature lower than -8 °C from 109 h/a to 37 h/a. This results in a saving of about 600 kWh/a and an increase in SPF from 2.65 to 2.74 (based on the climate data of the year 2016).
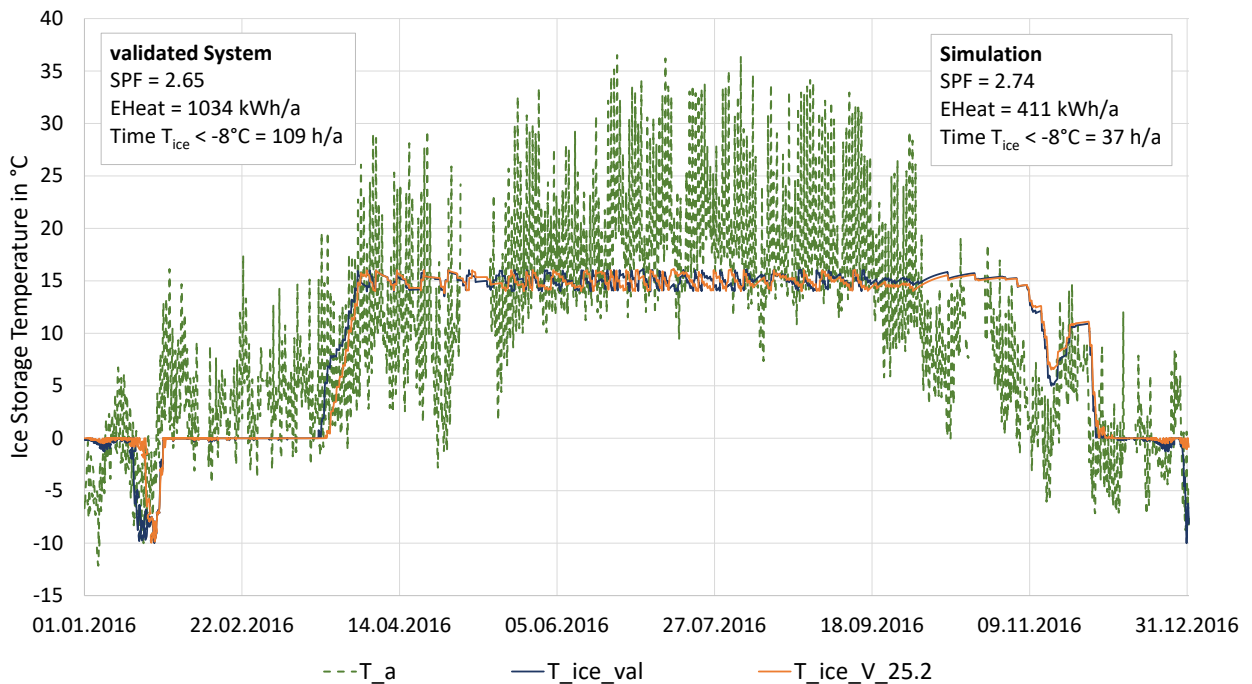
Figure 3-4: Ice storage temperature trend and key numbers for an ice storage volume of 25.2 m³
(Baseline: V_IS = 21 m³)

Figure 3-5 shows that an ice storage volume of about 30 m^3 would have prevented the subcooling completely in 2016, and the ice storage temperature drops only for a very short time below 0 °C and the SPF increases to 2.8. As shown in Figure 3-2 and Figure 3-4 a further increase of the ice storage volume has hardly any positive influence.
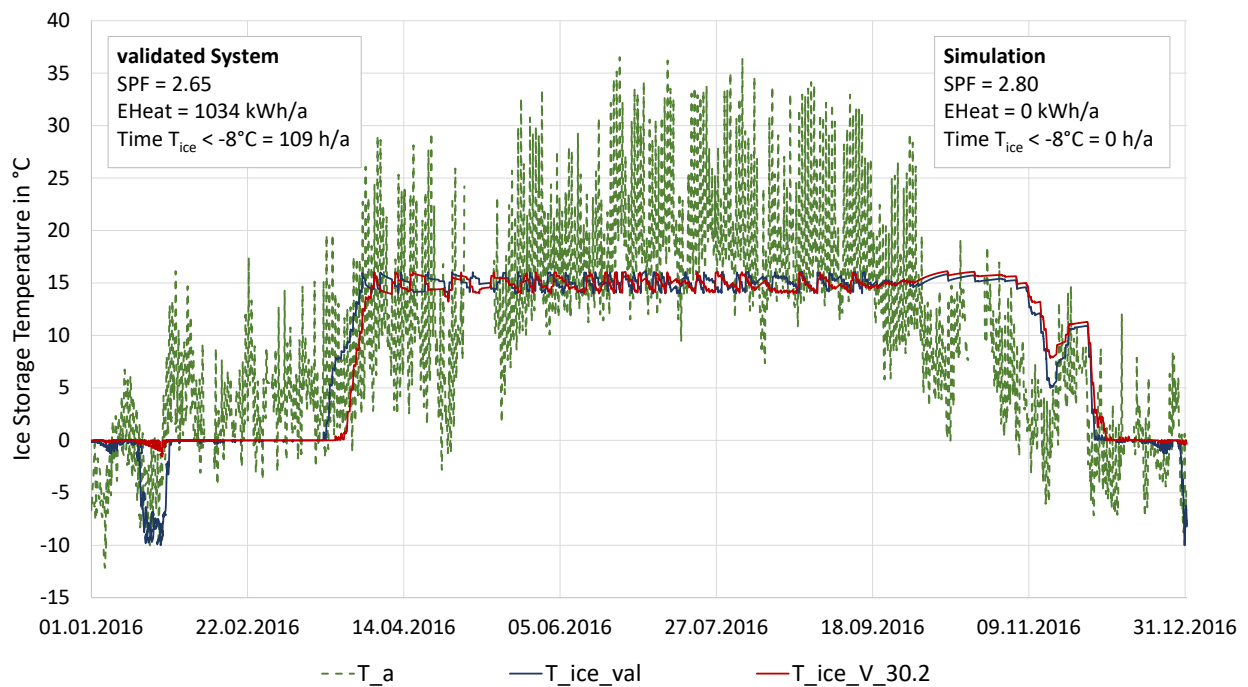
Figure 3-5: Ice storage temperature trend and key numbers for an ice storage volume of 30.2 m3 (Baseline: V_IS = 21 m^3)

In the following three figures, Figure 3-6 to Figure 3-8, the effect of the increase of the solar collector area is shown in more detail. With an increase of 20 % around 300 kWh/a of auxiliary heating can be saved, as it is shown in Figure 3-6. Moreover, it can be observed the lager the collector area is the earlier occurs the unfreezing of the storage.
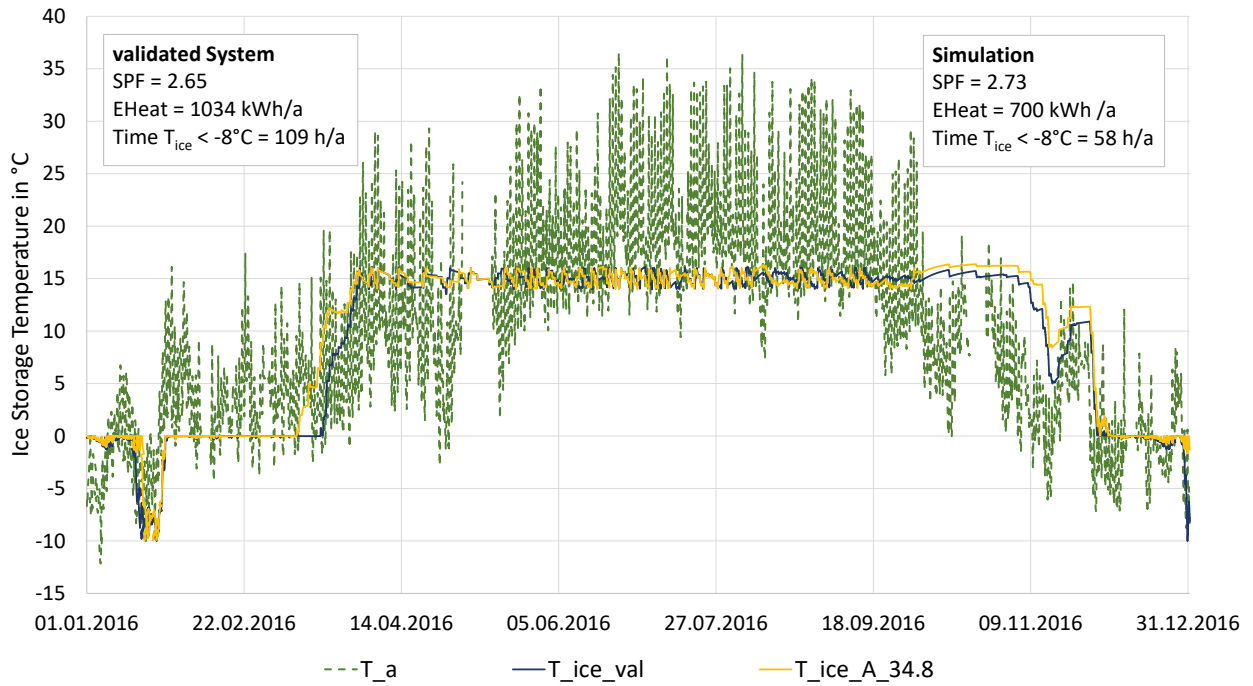
Figure 3-6: Ice storage temperature trend and key numbers for a collector area of 34.8 m2
(Baseline: A_Coll = 29 m²)

With an increase of the area from 29 m² to 50 m² around 700 kWh/a can be saved and the SPF is with 2.84 already higher than it is possible by increasing the ice storage volume only.
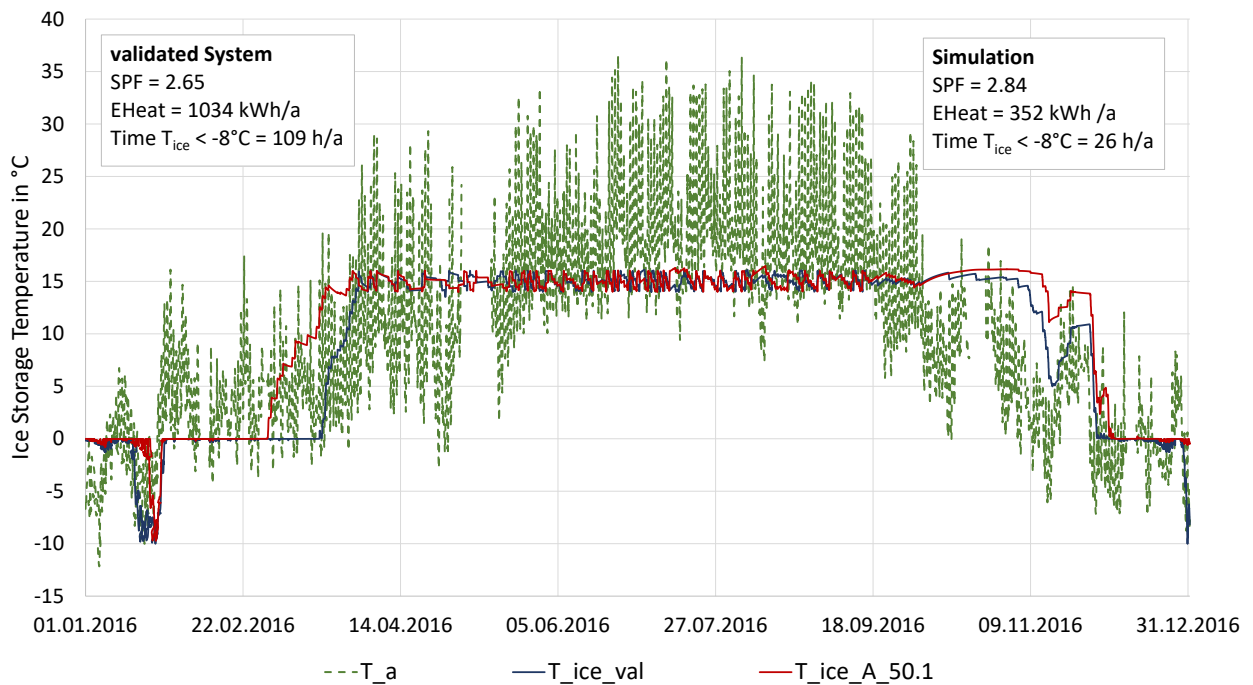
Figure 3-7: Ice storage temperature trend and key numbers for a collector area of 50.1 m²
(Baseline: A_Coll = 29 m²)

Figure 3-8 finally shows that the solar collector area has to be increased up to around 70 m² to avoid the subcooling completely for the climate data of 2016. This enlargement results in an SPF of 2.94. With a further enlargement of the collector area the SPF will still be increased but from the point on where no auxiliary heating is necessary anymore, a bigger increase of the collector area is necessary to achieve the same effect than before.
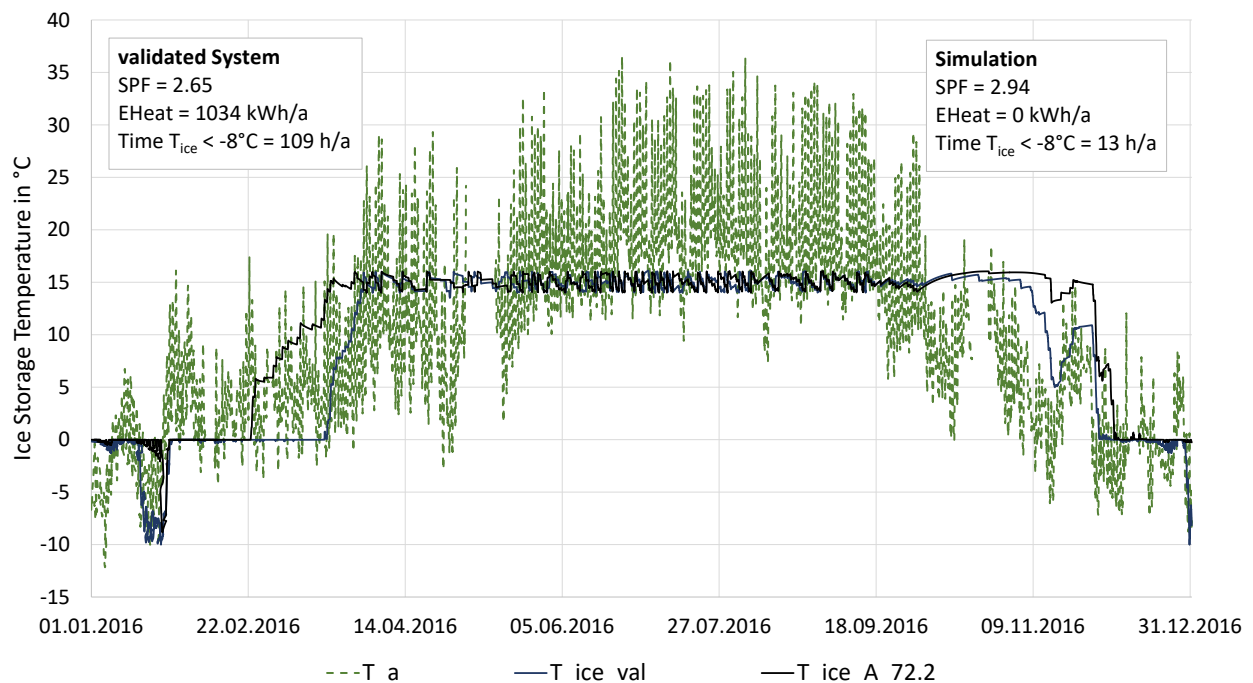
Figure 3-8: Ice storage temperature trend and key numbers for a collector area of 72.2 m2
(Baseline: A_Coll = 29 m²)

3.2 Variation of the collector angle of inclination

Here, the influence of the collector angle is examined. Currently the collector is installed with an angle of 10 °. It is shown that in the simulation model the increase of the inclination angle has hardly no influence. With an angle bigger than 25° the auxiliary heating decrease by about 100 kWh/a but the SPF remains nearly the same. According to the simulation model the variation of the collector angle is no suitable method for improving the system. However it is assumed that the influence is a bit bigger in the real system. That is because of some effects which are not simulated exactly because of the difference between the used simulation model and the actual installed collector. This issue is discussed in chapter *2.1.1 Validation of the single components.*

Moreover a steeper angle would have advantages regarding snow conditions. There have not been problems until now but there was not much snow in 2016 in Weiz. Since the SPF remains the same for different angles, it can be recommended to install the collector with a steeper angle to avoid such possible problems.
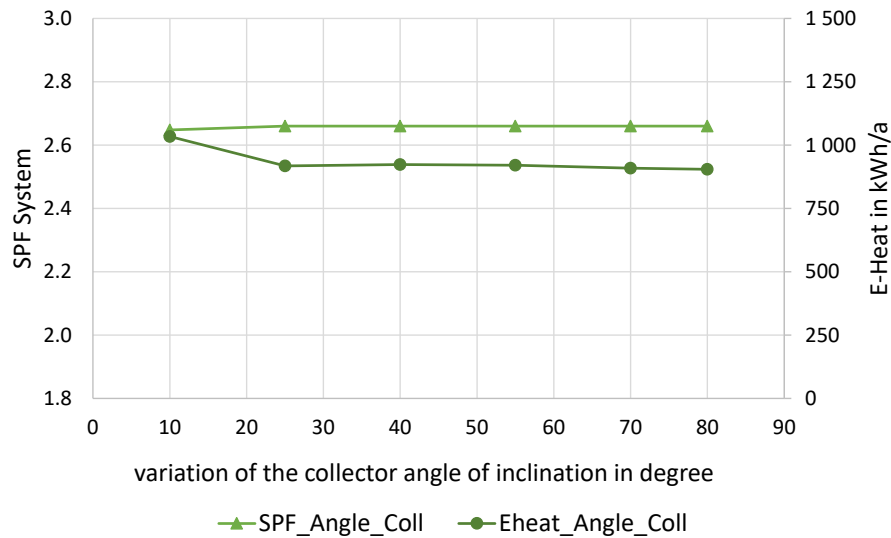
Figure 3-9: Sensitive analysis of the variation of the collector angle

However, according to the simulation model the influence of the collector angle on the ice storage temperature is negligible small.

3.3   Additional solar collector

This chapter deals with the influence of the installation of a second solar collector. The simulations have been carried out with a covered collector as well as with an evacuated tube collector. Furthermore, a distinction has been made according to the kind of integration. On the one hand the heating of the ice storage was examined and on the other hand the option of a direct DHW storage heating was evaluated too (compare Figure 3-10).
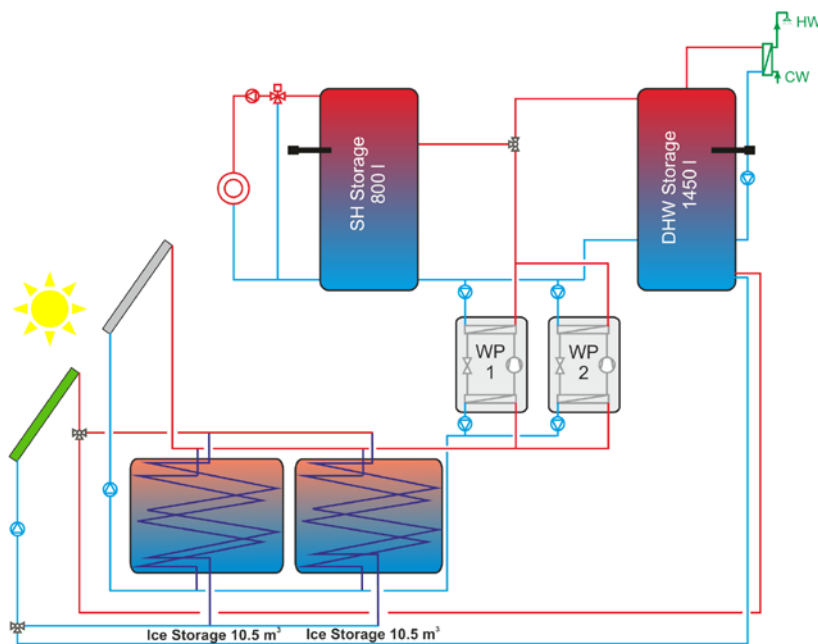
Figure 3-10: Scheme of the integration of an additional solar collector for ice storage regeneration and direct DHW heating

Figure 3-11 gives an overview of the simulation results for the different variants. One can see, with the evacuated tube collector in combination with DHW direct heating (without heat pump) the best SPF can be achieved, because the operating time of the two heat pumps can be significantly reduced during the summer months. For further details see Pratter (2017).
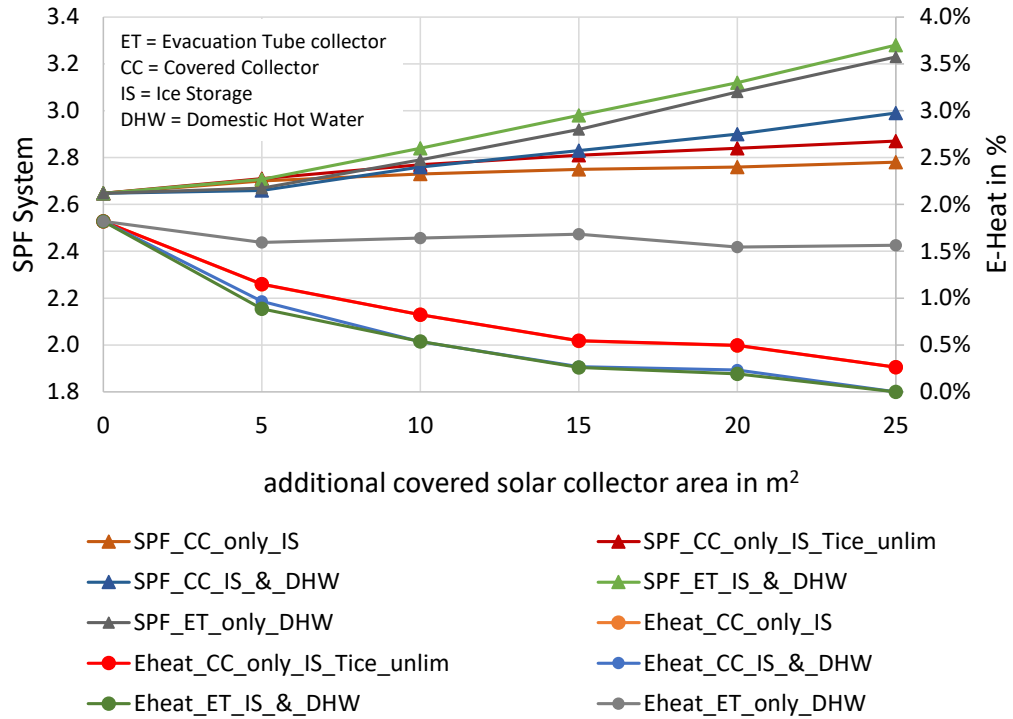
Figure 3-11: Sensitive analysis of different additional solar collectors with different integrations

4 Comparison of the solar-ice storage-heat pump system with an Air/Water heat pump

To allow a comparison of the ice storage system using brine/water heat pumps (BW-HP) to an air/water heat pump system (AW-HP), the same building was simulated using an air/water heat pump model. Figure 4-1 shows a schematic of this configuration. The system on the condenser side, i.e. heat sink side, is completely the same while the heat source system was replaced. Instead of two brine/water heat pumps using the ice storage and solar collector as heat source, the ambient air is used as heat source. Two identical air/water heat pumps are considered for a monovalent heat supply. Therefore, a heating capacity of 13.4 kW (A2/W35) per heat pump was assumed.
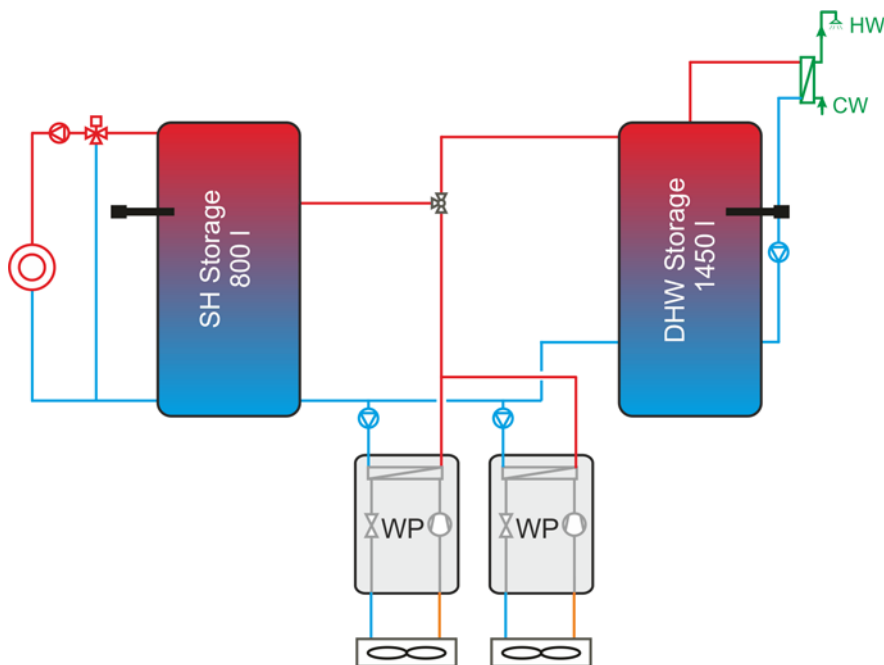
Figure 4-1: Schema of the Air/Water heat pump system

The simulation was carried out with a heat pump model generated by AIT. As described in the Austrian report on HPT Annex 50 – Task 3.1 (Austrian Task 3.1 report), for different refrigeration circuit configurations, numerical models were set-up within the simulation environment Dymola/Modelica. For the modelling of the heat pump components the TIL library[1] was used. A generic structure makes it possible to cover both the single stage refrigeration circuit and the more complex variants with EVI, i.e. vapour injection to the compressor at a middle pressure level, by simply activating or deactivating individual components (such as suction gas superheater, EVI injection, economizer) with a single model.

---

[1] https://www.tlk-thermo.com/index.php/de/software/til-suite

Here, the EVI configuration with R290 as refrigerant is considered and a charastic curve model (based on Dymola simulation results) have been used for the TRNSYS system simulations.

The characteristic curves are polynomial functions as follows**:**

$$\dot{Q}_H \text{ or } P_{el} = a + b \cdot x + c \cdot y + d \cdot z + e \cdot x^2 + f \cdot y^2 + g \cdot z^2 + h \cdot x \cdot y \cdot z \text{ [kW]} \qquad (4\text{-}1)$$

With   a to h… Constants (which are different for the calculation of the heating capacity ($\dot{Q}_H$) and for the electric power consumption of the compressor (P_{el}), see below).

   x…. $t_{sink,out}$ (delivery temperature in °C)

   y…. $t_{source,in}$ (outside air temperature °C)

   z…   Compressor speed (relative compressor speed in %)

For Task 3.2 the characteristic curve had to be adapted for a new building where additionally to space heating the domestic hot water operation is conducted by the heat pump. Therefore, the characteristic curve also needs to cover the domestic hot water operating points. The corresponding contants (a to h in Eq. (4-1)) can be found in Figure 4-2.

Here, the regression analysis still produces a feasible result, but due to the wider validity range, the quality of the fit decreases slightly. Especially for the electrical power consumption at low values, the regression model underestimates the prediction. However, as seen from the perspective of a yearly simulation, most of the operating points are in a range where the regression model predicts the values sufficiently reliable. For further details, see Austrian Task 3.1 report.
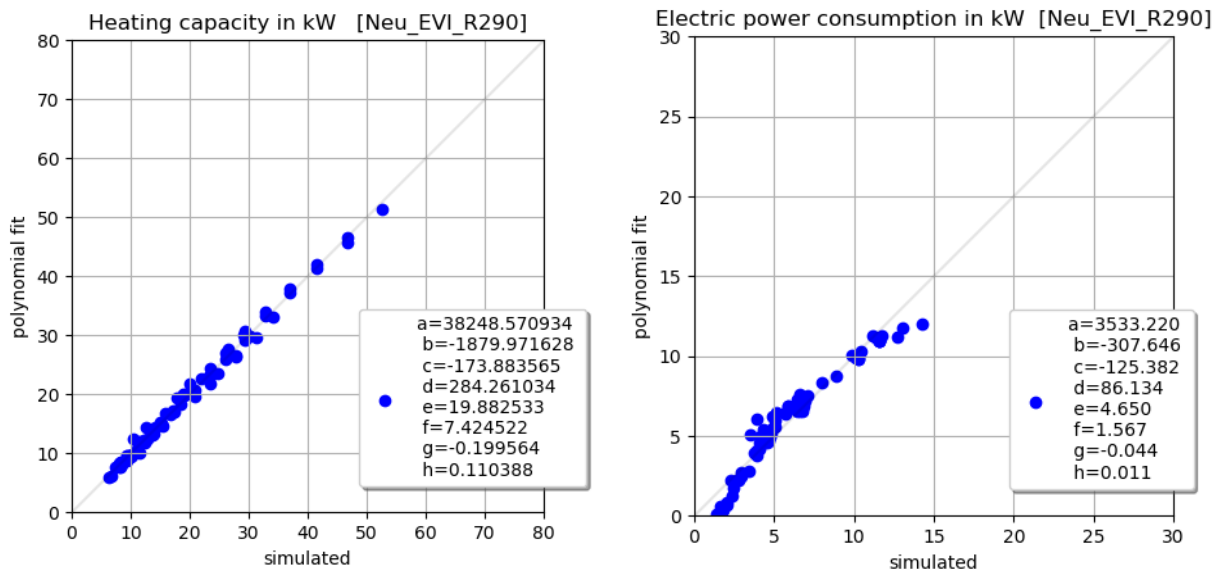
Input	Lower Limit	Upper Limit
T sink out °C	32	65
T source in °C	-10	12
Compressor speed in %	25	100

Figure 4-2: Polynomial fit vs. Dymola/Modelica simulation for EVI R290 (New building with domestic hot water included)

The efficiency values of this air/water heat pump are in the top range of the currently available air-water heat pumps. The most important technical specifications of both the brine/water heat pump (ice storage system) and the air/water heat pump are shown in Table 4-1.

Table 4-1: Specifications of the installed brine/water heat pumps (BW-HP) in comparison to the modelled air/water heat pump (AW-HP)

	Case BW-HP & Ice Store				Case AW-HP	
	HP1 - B0/W35	HP1 - B0/W50	HP2 - B0/W35	HP2 - B0/W50	HP1&2- A2/W35	HP1&2- A2/W50
Heating capacity [kW]	5.9	3.5	10.1	6.1	13.4	7.8
COP [-]	4.51	2.50	4.72	2.88	4.41	3.64

Results of the annual simulations with the solar/ice-storage heat pump system and the air/water heat pumps are shown in Figure 4-3. As one can see, the system efficiency of the ice storage system is lower than the efficiency of the system with the air/water heat pumps. The "BW-HP & Ice Storage" reaches a SPF_{sys} of 2.67, and the simulated system with air/water heat pumps 2.85. In both cases, the SPF has been determined according to equation (2-7).

However, due to the low heating capacity in the case of hot water preparation and the relatively high hot water demand, an electric heater for hot water preparation is necessary to compensate for short-term demand peaks. Therefore, the overall electrical energy demand (see Figure 4-6) covers the heat pumps, the auxiliary heating (electric cartridge) and the consumption of the circulation pumps on the heat sink side incl. the heat distribution system.
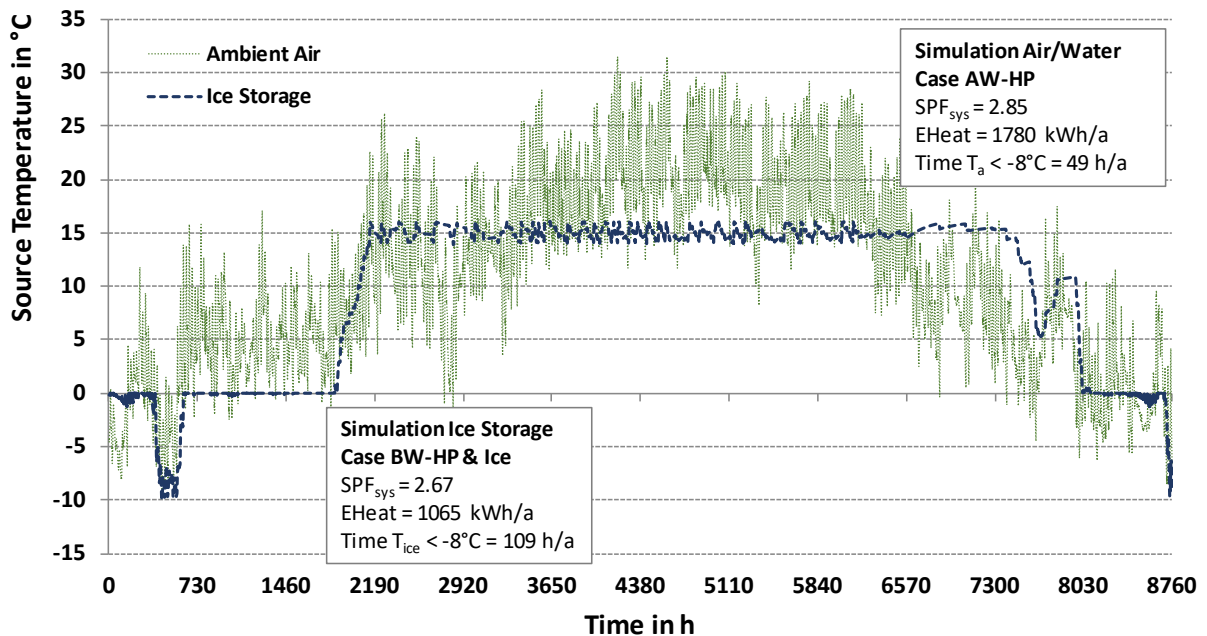
Figure 4-3: Source temperatures of the BW-HP (Ice-Storage temperature) versus AW- HP (Ambient Air temperature) and key data for the two systems

Figure 4-4 shows the cumulative lines of the heating load, as well as the supply and return flow temperature of the two air-to-water heat pumps. On the one hand, this diagram shows the typical temperature range of room heating (30 - 35 °C) and hot water preparation (55 - 64 °C) and on the other hand, the heat output delivered to the condenser is shown as the sum of the two heat pumps.
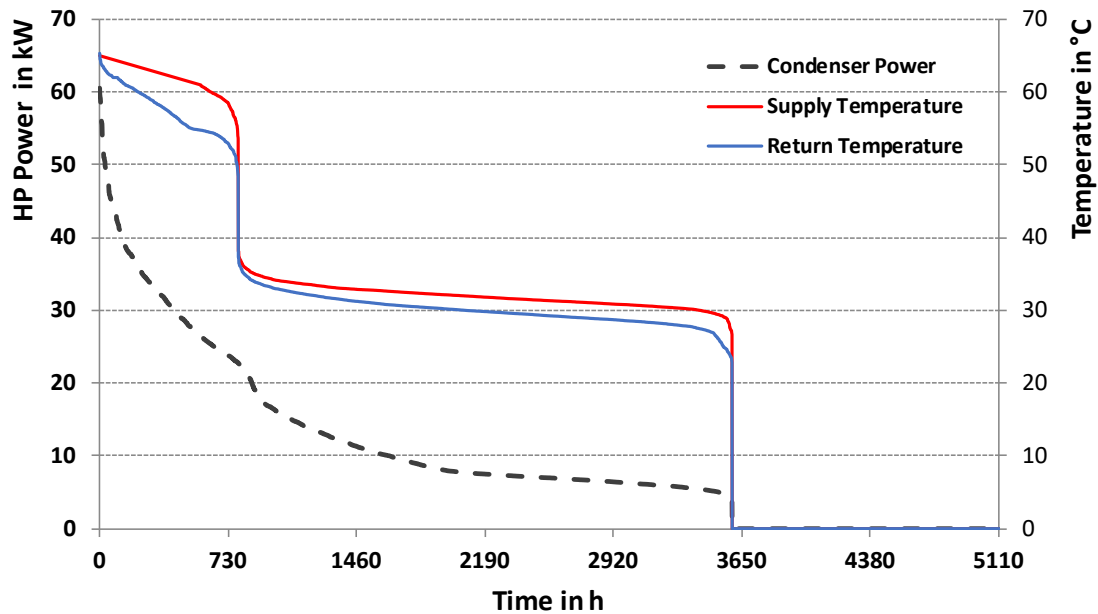
Figure 4-4: Annual duration curves of the condenser capacity, the flow and return temperature of the air to water heat pumps

More detailed results are summarized in Figure 4-5. On the input side, the heat delivered by the electrical heaters (Q_aux) and the amount of heat supplied by the heat pumps (Q_HP) are shown. The output is separated in hot water supply (Q_DHW), space heat demand (Q_SH) and system losses (Q_losses).

On the one hand the system losses of the ice storage system are higher than in the case of the air/water heat pump. On the other hand, the electricity consumption of the E-cartridge in the domestic hot water storage is higher in case of the AW-HP due to the low heating capacity of the heat pumps at high flow temperatures.
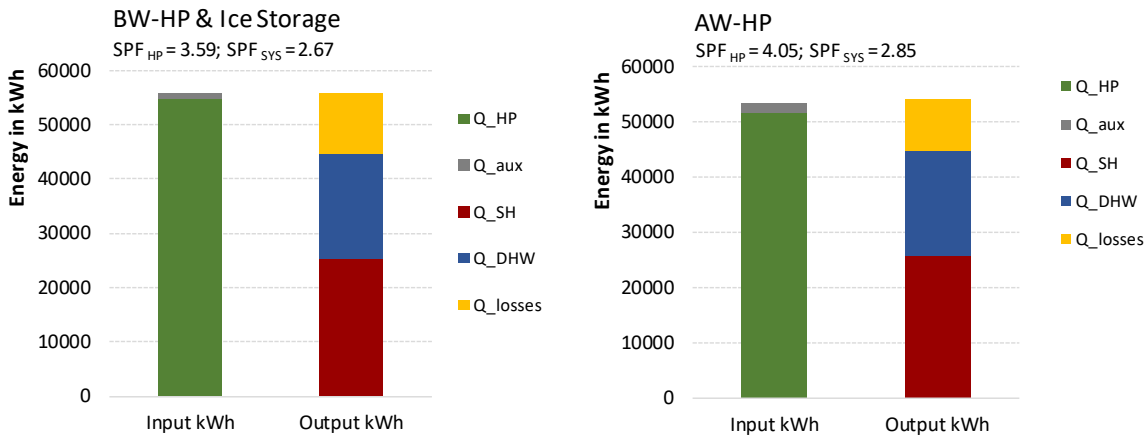
Figure 4-5: Balance sheets – case BW-HP with Ice Storage versus case AW-HP

The electricity consumption of the two heat pump systems is shown in Figure 4-6. In addition to the electricity that is directly converted into heat (Q_aux), the electricity demand of the heat pump (E_HP) and the necessary pumps (E_Pumps) is shown.

The slightly lower SPF of the BW-HP results in a higher electricity demand of the heat pumps, while for the AW-HP system it is noticeable that the E-cartridge is needed more often.
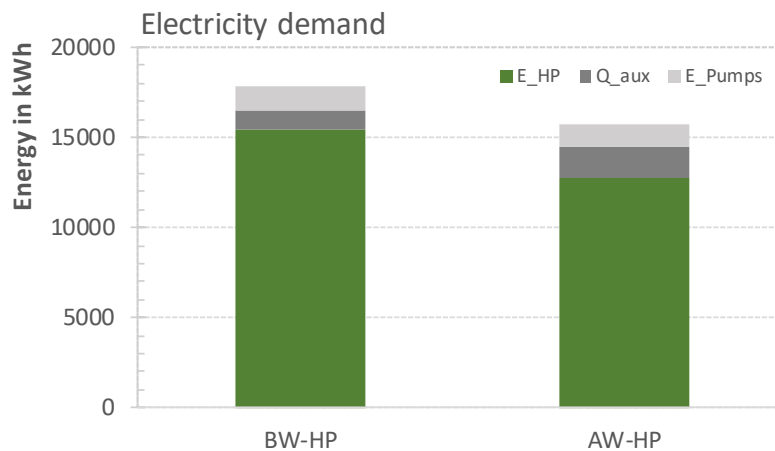
Figure 4-6 Balance sheet electricity demand– case BW-HP with Ice Storage versus case AW-HP

Figure 4-7 shows the monthly SPF's of the two cases considered. One can see, that the BW-HP achieves almost a constant SPF over the whole year. The SPF ranges between 3.4 and 3.8. Over the year, a SPF of 3.6 is achieved.

The AW-HP, on the other hand, shows clear variations over the months. In the summer months (dominated by domestic hot water heating) the SPF is at the same level (3.6 - 3.7) as the BW-HP achieves. In the transition period (high space heating energy demand with moderate outside air temperature), significantly higher SPFs (4.2 – 5.2) can be achieved (see also Figure 4-3). Only in the

coldest months, because of the low ambient air temperatures the AW-HP achieve SPFs (3.6 – 3.7) comparable to that of the BW-HP.
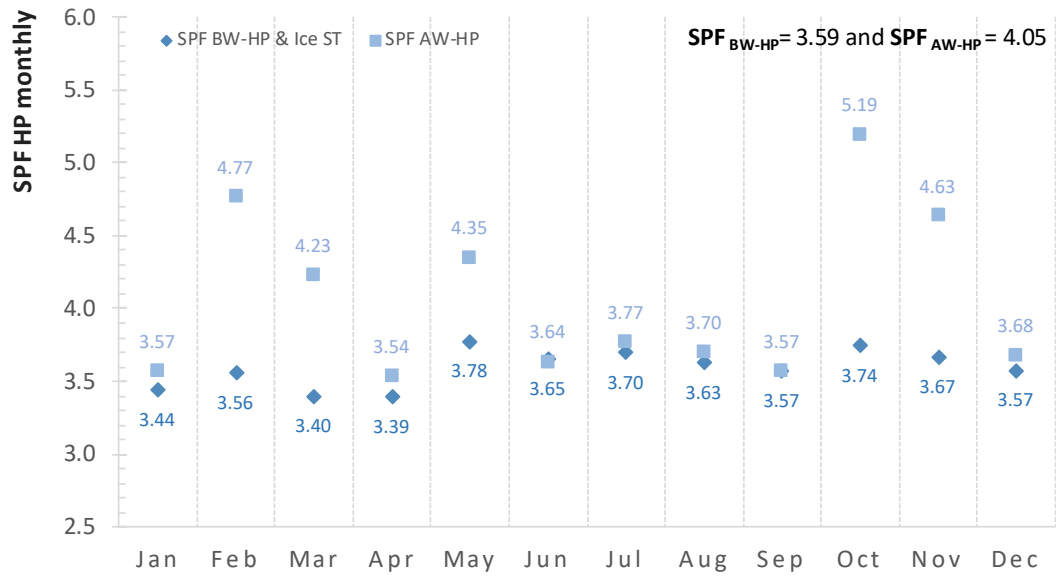
Figure 4-7: Monthly values of the SPF of both heat pump types (BW- & AW-HP)

5   Conclusions

Based on the monitoring results a TRNSYS model for the heating system of an existing multi family building located in Weiz (Austria) has been set up. The heating system uses an ice storage and solar collectors as heat source for two brine/water heat pumps. The comparisons of measured and simulated data are sufficiently accurate, although some deviations occurred. Thus, the model can be used for simulation studies, e.g. dealing with the effect of varying the ice storage volume or/and the collector area.

Basically, the much higher space heating and domestic hot water (DHW) demand – in comparison to the initially assumed design data according to the energy certificate – resulted in an under dimensioning of the heat sources.

As shown by means of simulations, the performance of the existing system could be increased by an enlargement of the solar collector area and/or the ice storage volume, thus no subcooling of the ice storage occurs. However, with a larger solar collector area a higher SPF can be reached.

Moreover, it can be concluded that a significant increase of the SPF is possible by enabling a direct DHW heating with an additional solar collector. This is a very interesting aspect for improving the system in Weiz, because the installation would be relatively easy.

The comparison of the ice storage system using brine/water heat pumps with air/water heat pumps shows, that it is possible to reach higher SPFs with an "optimized" air/water heat pump than with the currently used brine/water heat pumps using an ice storage and solar collectors as heat source. However, one must consider that still some room for improvements exist with respect to storage volume, and solar collector as well as direct preparation of hot water via the solar collectors. Furthermore, the considered brine/water heat pumps do not represent the most efficient products on the market, while the data for the air/water heat pumps are based on an advanced refrigerant circuit with vapour injection and propane as refrigerant. So far, no closer financial analysis of the systems has been carried out, but one can assume, that the ice storage system is more expensive than the "advanced" air/water heat pumps.

It should be noted that all the key figures discussed in this report are based on climate data of 2016 meausered in Graz. I.e., the numbers will differ for different climate data.

6 References

Cao, S.; Siren, K.; Heinz, A; Bonk, S. 2013. Models of Sub-Components and Validation for the IEA SHC Task 44 / HPP Annex 38 . http://iea-shc.org/data/sites/1/publications/

T44A38_Rep_C2_E_Storage_Final_Draft.pdf. 2013.

Claußen, T. 1993. Entwicklung und experimentelle Verifizierung eines dynamischen Latentwärmespeichermodells. Universität Oldenburg : Diplomarbeit am Studiengang Diplom-Physik, 1993.

Gutensohn, R. 2012. Viessmann Eisspeichersystem - Ein neues Versorgungskonzept. [Online] 2017 [Zitat vom: 06. 04 2017.] http://www.fws.ch/tl_files/download_d/Downloads/Gutensohn-FWS%20%2011_2012%20Eisspeicher.pdf.

Hackl, R. 2016. Analyse einer realen Eisspeicher - Wärmepumpenanlage mit Solar - Luftkollektoren. Graz : Technische Universität Graz - Institut für Wärmetechnik: Bachelorarbeit, 2016.

Halozan, H und Holzapfel, K. 1987. Heizen mit Wärmepumpen; TÜV Rheinland; Köln,1987.

Heimrath, R. 2004. Simulation, Optimierung und Vergleich solar thermischer Anlagen zur Raumwärmenutzung für Mehrfamilienhäuser. Graz : PhD thesis, Institute of Thermal Engineering, TU Graz, 2004.

Heinz, A. 2015. Wärmespeicher Päsentation zur Vorlesung Sonnenenergienutzung. Graz : TU Graz, 2015.

HMI-Master GmbH. 2017. Homepage [Online] 2017. [Zitat vom: 06. 04 2017.] http://www.hmi-master.at/.

HOT ICE. 2017. Photos taken during the project HOT ICE. http://www.innovationszentrum-weiz.at/veranstaltungen-aktuelles/detail/projekt-hot-ice. Weiz.

Hutter, G. 2016. Foto Gebäude Weiz; per E-Mail zur Verfügung gestellt. Weiz : SG ELIN Weiz, 2016.

IAE SHC. 2017. SHC Task 44 - Solar and Heat Pump Systems. [Online] 2017.

[Zitat vom: 03. 04 2017.] http://task44.iea-shc.org.

ISFH. 2011. Modell eines unverglasten photovoltaisch-thermischen Sonnenkollektors für TRNSYS 16. Emmerthal, 2011.

Institute of Thermal Engineering. 2017. https://www.tugraz.at/en/institutes/iwt/home/. Graz : TU Graz, 2017.

Janßen Energieplanung. 2010. Type 708 für TRNSYS 16. Hannover, 2010.

Kummert, M. 2007. Using GENOPT with TRNSYS 16 and type 56. Glasgow : ESRU – University of Strathclyde, 2007.

Landis+Gyr. 2017. T550 Ultraheat. [Online] 2017. [Zitat vom: 06. 04 2017.] http://www.landisgyr.com/webfoo/wp-content/uploads/2013/06/Landis+Gyr-T550-UC50_Projektierungsanleitung.pdf.

Lerch, W. 2017. Combined Solar/Heat Pump-System, Draft (unpublished) thesis, TU Graz - Institute of Thermal Engineering, 2017.

Lerch, W.; Heimrath, R. und Heinz, A. 2016. Direct use of solar energy as heat source for a heat pump in comparison to a conventional parallel solar air heat pump system. Graz : University of Technology Graz, Institute of Thermal Engineering, 2016. http://www.sciencedirect.com/science/article/pii/S037877881500198X

Pratter, R. 2017. Validation of a solar-ice storage-heat pump system and definition of a design guideline, Master Thesis, Graz University of Technology – Institute of Thermal Engineering.

Pratter, R.; Lerch W.; Heimrath R.; et al. (2017). Latentwärmenutzung mit Eisspeicher, Wärmepumpe, Solarthermie und PV-Anlage – Systemevaluierung, Systemoptimierung und Dimensionierungsrichtlinie, Project report submitted to the province of Styria, Graz University of Technology – Institute of Thermal Engineering.

TB Bierbauer GmbH. 2015. Schautafel HotIce Weiz. 2015. Kontakt: http://www.bierbauer-tb.at/index.php/kontakt.

TESS (2012). TESSLibs 17: Component Libraries for the TRNSYS Simulation Environment. Thermal Energy Systems Specialists (TESS), Madison Wisconsin, USA.

TRNSYS. 2012. TRNSYS 17 User Manual. Madison Wisconsin, USA : Solar Energy Laboratory (SEL), University of Wisconsin, 2012.

VDI Wärmeatlas. 1997. Wärmeübergang und Strömung in Verfahrenstechnik und Chemie, 8. Auflage. Springer Verlag, 1997.

Visser, H. 1986. Energy Storage in Phase Change Materials, Development of a component model compatible with the TRNSYS transient simulation program. Delft University of Technology : Department Applied Physics, 1986.

ZAMG. 2017. Erfassung der Klimadaten am Standort Inffeldgasse, Graz, im Zuge des Projekts: MPC-Box - Model Predictive Control of thermal activated Building Components and Measurements in Test-Boxes. https://online.tugraz.at/tug_online/fdb_detail.ansicht?cvfanr=F33110&sprache=2. Österreich, 2017.

Appendix - Schematics of the system in Weiz
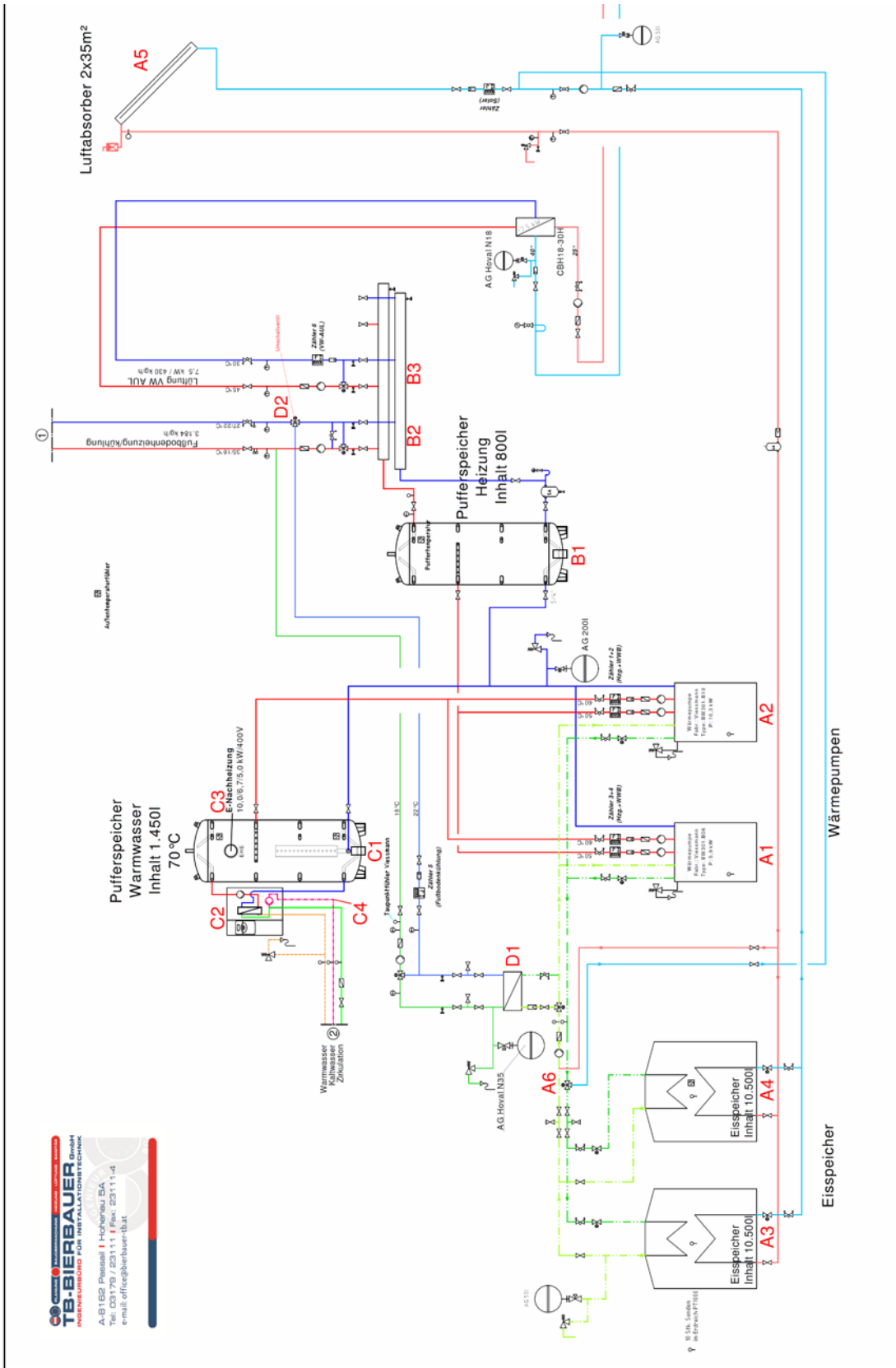
Figure A- 1: Measurement scheme (TB Bierbauer GmbH, 2015)